National Aeronautics and
Space Administration

Dryden Flight Research Center
P.O. Box 273
Edwards, California 93523-0273

Reply to
Attn of: Dryden Technical Publications April 1, 2004

TO: All Holders of NASA/TP-2003-212034, Dated December 2003

FROM: T/Technical Publications Office

SUBJECT: Errata Sheet for NASA/TP-2003-212034, Dated December 2003

NASA/TP-2003-212034, *Aging Theories for Establishing Safe Life Spans of Airborne Critical Structural Components*, by William L. Ko has an error in table 2 on page 14. Please make the following changes to this document.

1. Delete the current text on page 14.
2. Insert the new attached page 14 with the corrected column C in table 2.
3. Staple the errata sheet to the inside front cover of the document.

Thank you for your cooperation.

Michael H. Gorn
Acting Chief of Code T

Attachment
as stated

$$(\sigma_{\max})^m\left(1-\frac{\sigma_s}{\sigma_{\max}}\right)^n = \frac{(2)^{1-n}}{C(m-2)}\left(\frac{1}{AM_k}\sqrt{\frac{Q}{\pi}}\right)^m \frac{\left(a_c^p\right)^{1-\frac{m}{2}} - \left(a_1\right)^{1-\frac{m}{2}}}{N_1} \tag{45}$$

In equation (45), the right-hand side is known, and the left-hand side has two unknowns: $\sigma_{\max}$ and σ_s. Thus, there are multiple combinations of $\sigma_{\max}$ and σ_s for finding the equivalent-constant-amplitude load spectrum. The most practical way is to choose the value of the mean stress σ_s of the random loading spectrum by inspection, and then calculate the equivalent maximum stress $\sigma_{\max}$ from equation (45).

NUMERICAL EXAMPLE

The numerical example is to demonstrate how to calculate the number of safe flights for a flight test program. The example chosen is the NASA B-52B carrier aircraft pylon hooks (one front hook, two rear hooks) (figs.1, 2) carrying the Pegasus winged three-stage solid rocket (44,629 lb) up to high altitude (approximately 40,000 ft) for air-launching, firing and sending the payload into orbit.

Material Properties

The material properties of the B-52B pylon front and rear hooks are listed in table 2.

Table 2. Material properties of B-52B pylon hooks.

Part name	Material	σ_U ksi	σ_Y ksi	τ_U ksi	K_{I_C} ksi$\sqrt{\text{in.}}$	C $\frac{\text{in.}}{cycle}(\text{ksi}\sqrt{\text{in.}})^{-\text{m}}$	m	n
Front hook	Inconel 718*	175	145	135	125	9.220×10^{-12}	3.60	2.16
Rear hooks	AMAX MP35N†	250	235	141	124	2.944×10^{-11}	3.24	1.69

* Inco Alloys International, Inc., Huntington, West Virginia.
† H. C. Starck, Inc., Cleveland, Ohio.

Input Crack Data

The fictitious surface crack at the critical stress point of each hook is assumed to be semicircular in shape ($c = a$, fig. 14). This is based on the observations of the past failed B-52B pylon two rear hooks. The crack propagation initiation sites of the failed hooks were almost semi-circular surface cracks of depths a = 0.031 in. and a = 0.038 in. respectively for the inboard and outboard hooks (ref. 2). Note from figure 14 that the semicircular surface crack has the relatively high value of Q. Other crack parameters used were: A = 1.12 for the surface crack, and M_K = 1.0 for the high (hook depth) to (crack depth) ratios.

NASA/TP-2003-212034

Aging Theories for Establishing Safe Life Spans of Airborne Critical Structural Components

William L. Ko
NASA Dryden Flight Research Center
Edwards, California

December 2003

The NASA STI Program Office…in Profile

Since its founding, NASA has been dedicated to the advancement of aeronautics and space science. The NASA Scientific and Technical Information (STI) Program Office plays a key part in helping NASA maintain this important role.

The NASA STI Program Office is operated by Langley Research Center, the lead center for NASA's scientific and technical information. The NASA STI Program Office provides access to the NASA STI Database, the largest collection of aeronautical and space science STI in the world. The Program Office is also NASA's institutional mechanism for disseminating the results of its research and development activities. These results are published by NASA in the NASA STI Report Series, which includes the following report types:

- TECHNICAL PUBLICATION. Reports of completed research or a major significant phase of research that present the results of NASA programs and include extensive data or theoretical analysis. Includes compilations of significant scientific and technical data and information deemed to be of continuing reference value. NASA's counterpart of peer-reviewed formal professional papers but has less stringent limitations on manuscript length and extent of graphic presentations.

- TECHNICAL MEMORANDUM. Scientific and technical findings that are preliminary or of specialized interest, e.g., quick release reports, working papers, and bibliographies that contain minimal annotation. Does not contain extensive analysis.

- CONTRACTOR REPORT. Scientific and technical findings by NASA-sponsored contractors and grantees.

- CONFERENCE PUBLICATION. Collected papers from scientific and technical conferences, symposia, seminars, or other meetings sponsored or cosponsored by NASA.

- SPECIAL PUBLICATION. Scientific, technical, or historical information from NASA programs, projects, and mission, often concerned with subjects having substantial public interest.

- TECHNICAL TRANSLATION. English-language translations of foreign scientific and technical material pertinent to NASA's mission.

Specialized services that complement the STI Program Office's diverse offerings include creating custom thesauri, building customized databases, organizing and publishing research results…even providing videos.

For more information about the NASA STI Program Office, see the following:

- Access the NASA STI Program Home Page at ***http://www.sti.nasa.gov***

- E-mail your question via the Internet to help@sti.nasa.gov

- Fax your question to the NASA Access Help Desk at (301) 621-0134

- Telephone the NASA Access Help Desk at (301) 621-0390

- Write to:
  NASA Access Help Desk
  NASA Center for AeroSpace Information
  7121 Standard Drive
  Hanover, MD 21076-1320

NASA/TP-2003-212034

Aging Theories for Establishing Safe Life Spans of Airborne Critical Structural Components

William L. Ko
NASA Dryden Flight Research Center
Edwards, California

National Aeronautics and
Space Administration

Dryden Flight Research Center
Edwards, California 93523-0273

December 2003

NOTICE

Use of trade names or names of manufacturers in this document does not constitute an official endorsement of such products or manufacturers, either expressed or implied, by the National Aeronautics and Space Administration.

Available from the following:

NASA Center for AeroSpace Information (CASI)
7121 Standard Drive
Hanover, MD 21076-1320
(301) 621-0390

National Technical Information Service (NTIS)
5285 Port Royal Road
Springfield, VA 22161-2171
(703) 487-4650

CONTENTS

Page

ABSTRACT 1

NOMENCLATURE 1

INTRODUCTION 3

B-52B LAUNCH AIRCRAFT PYLON HOOKS 4

CONVENTIONAL AGING THEORY 5

CRACK GROWTH CALCULATIONS 6

EQUIVALENT-CONSTANT-AMPLITUDE AGING THEORIES 7
- Discrete Aging Theory 8
  - 1. Crack Growth 8
  - 2. Number of Safe Flights 10
- Closed-Form Aging Theory 10
  - 1. Crack Growth 10
  - 2. Number of Safe Flights 12

EQUIVALENT STRESS AMPLITUDES 13

NUMERICAL EXAMPLE 14
- Material Properties 14
- Input Crack Data 14
- Equivalent-Constant-Stress Amplitudes 15
- Number of Safe Flights 16

CONCLUDING REMARKS 17

APPENDIX 18

KO FIRST-ORDER AND KO SECOND-ORDER AGING THEORIES 18
- Ko First-Order Aging Theory 19
- Ko Second-Order Aging Theory 19

REFERENCES 21

FIGURES 22

ABSTRACT

New aging theories have been developed to establish the safe life span of airborne critical structural components such as B-52B aircraft pylon hooks for carrying air-launch drop-test vehicles. The new aging theories use the "equivalent-constant-amplitude loading spectrum" to represent the actual random loading spectrum with the same damaging effect.

The crack growth due to random loading cycling of the first flight is calculated using the half-cycle theory, and then extrapolated to all the crack growths of the subsequent flights.

The predictions of the new aging theories (finite difference aging theory and closed-form aging theory) are compared with the classical flight-test life theory and the previously developed Ko first- and Ko second-order aging theories. The new aging theories predict the number of safe flights as considerably lower than that predicted by the classical aging theory, and slightly lower than those predicted by the Ko first- and Ko second-order aging theories due to the inclusion of all the higher order terms.

NOMENCLATURE

A	crack location parameter
a	depth of semi-elliptic surface crack, in.
a_c^o	operational limit crack size, in.
a_c^p	initial fictitious crack size established by proof load test, in.
a_l	crack size at the end of the l-th flight, in.
C	material constant in Walker crack growth rate equation, $\frac{\text{in.}}{\text{cycle}}(\text{ksi}\sqrt{\text{in.}})^{-\text{m}}$
c	half length of surface crack, in.
E	complete elliptic function of the second kind
F_1	number of safe flights at the first flight
$\bar{F}_1$	number of safe flights based on Ko first-order aging theory
$\tilde{F}_1$	number of safe flights based on Ko second-order aging theory
F^*	number of safe flights based on Ko discrete aging theory
F_1^*	number of safe flights based on Ko closed-form aging theory
f	fraction of proof load (f < 1)
ksi	kilopounds
K_{I_C}	mode I critical stress intensity factor, ksi$\sqrt{\text{in}}$.
$K_{\max}$	mode I stress intensity factor associated with $\sigma_{\max}$, ksi$\sqrt{\text{in}}$.
ΔK	mode I stress intensity amplitude, ksi$\sqrt{\text{in}}$.
i, j	= 1, 2, 3, . . . , integers associated with the i-th, or j-th half cycle
k	modulus of elliptic function

l	= 1, 2, 3, . . . , integer associated with the *l*-th flight
M_k	flaw magnification factor
m	Walker exponent associated with maximum stress $\sigma_{\max}$, or stress amplitude $(\sigma_{\max} - \sigma_{\min})$
N_l	number of stress cycles consumed during the *l*-th flight
N_{total}	total number of stress cycles allowed for safe flights
n	Walker exponent associated with stress ratio *R*
Q	surface flaw and plasticity factor
R	stress ratio, $R = \sigma_{\min} / \sigma_{\max}$
SRB/DTV	solid rocket booster/drop test vehicle
V_A	front hook load, lb
V_{BL}	left rear hook load, lb
V_{BR}	right rear hook load, lb
V_A^p	front hook proof load, lb
V_{BL}^p	left rear hook proof load, lb
V_{BR}^p	right rear hook proof load, lb
Δa_l	amount of crack growth induced by the *l*-th flight, in.
δa_i	crack growth induced by the *i*-th half cycle, in.
θ_c	angular location of critical stress point measured from horizontal axis, degree
σ_1	tangential stress at critical stress point of front hook, ksi
σ_2	tangential stress at critical stress point of left rear hook, ksi
σ_3	tangential stress at critical stress point of right rear hook, ksi
σ^*	$= \sigma_1^*$ or σ_2^* or σ_3^*, ksi
σ_1^*	value of σ_1 associated with V_A^p, ksi
σ_2^*	value of σ_2 associated with V_{BL}^p, ksi
σ_3^*	value of σ_3 associated with V_{BR}^p, ksi
σ_U	ultimate tensile stress, ksi
σ_Y	yield stress, ksi
$\sigma_{\max}$	maximum stress, ksi
$\sigma_{\min}$	minimum stress, ksi
σ_s	mean stress, ksi
σ_t	tangential stress at hook inner boundary, ksi
$(\sigma_t)_{max}$	maximum value of σ_t, ksi

τ_U ultimate shear stress, ksi

$(\ )_i$ quantity associated with the *i*-th stress half cycle

$(\ )_l$ quantity associated with the *l*-th flight

ϕ angular coordinate for semi-elliptic surface crack, rad

INTRODUCTION

The NASA Dryden Flight Research Center (DFRC) B-52B launch aircraft has been used to carry various types of research vehicles by means of pylon hooks for high-altitude air-launch tests. The past air-launch vehicles include the following drop-test vehicles: the X-15 rocket plane (35,250 lb without drop tanks; 51,600 lb with drop tanks); HL-10 lifting body (15,380 lb); highly maneuverable aircraft technology (HiMAT) vehicle (3,528 lb with 4,000 lb adapter); the drone for aerodynamic and structural testing (DAST) vehicle (2,500 lb with 4,000 lb adapter); the solid rocket booster/drop test vehicle (SRB/DTV) (49,000 lb); Pegasus (Orbital Sciences Corp., Fairfax, Virginia) winged rocket (44,629 lb including 2,400 lb adapter); and X-38 drop test vehicle (18,100 lb). Each of the test vehicles is attached to the B-52B aircraft pylon through one L-shaped front hook and two identical rear hooks with the exception of the X-38. (The X-38 case used one front hook and one rear hook of a different pylon (ref. 1).) The L-shaped hook geometry will always induce tangential tensile stress concentration at the hook's inner curved boundary, which is the potential fatigue-crack initiation site.

During the early stages of the SRB/DTV flight test program, the two old rear hooks (4340 steel) failed almost simultaneously during towing of the B-52B carrying the SRB/DTV on a relatively smooth taxiway (low-amplitude dynamic loading) after cancellation of the drop test due to unfavorable weather. Careful examination of the fracture surface of each failed old rear hook revealed that each hook had an existing microsurface crack at the critical stress points from where the microcrack rapidly propagated, resulting in the hook failure (ref. 2). The surface microcrack could have been initiated from the previous long period of flight-test stress cycling and surface corrosion. Had the hook failed during the takeoff run or during the captive flight, a catastrophic accident might have occurred. The potential for this type of accident underscores the need for reliable and accurate predictions of the fatigue life of pylon hooks.

Using the half-cycle theory (ref. 3), Ko (refs. 4, 5) calculated the amount of crack growth at the critical stress point of each hook for each test flight using the actual random loading spectrum. Then, with certain assumptions, the Walker crack-growth equation was applied to formulate Ko first-order (ref. 5) and Ko second-order aging theories (refs. 6, 7) for predicting the number of remaining flights for the safe flight tests. Those theories predicted far fewer safe flights than those calculated from the classical aging theory. The Ko theories, however, were found to lose accuracy as the number of flights increases due to the neglected higher-order terms which become larger due to growing crack size.

The safety of flight tests using aircraft pylon hooks to carry any drop-test vehicle hinges upon the structural integrity of the pylon hooks. It is, therefore, of vital importance to develop highly accurate aging theories to set the limit of safe flight-test life span for airborne critical structural components such as B-52B aircraft pylon hooks. This report presents two new aging theories for establishing the safe flight-test life span of B-52B hooks. The results are compared with the earlier Ko first- and Ko second-order aging theories, and also with the conventional aging theory for predicting the number of safe flights.

B-52B LAUNCH AIRCRAFT PYLON HOOKS

Figure 1 shows the B-52B aircraft pylon carrying a particular store of Pegasus winged rocket through one front hook and two identical rear hooks before takeoff. Figure 2 shows the geometry of the front and rear hooks, with the location of the critical stress point for each hook indicated. Figures 3 and 4, respectively, show the tangential tensile stress distributions along the inner boundaries of the front and rear hooks calculated from the finite-element linear elasticity analysis (ref. 2). Note the tangential stress concentration at the critical stress point of each hook. Based on the finite-element stress analyses, the relationships between the hook loads $\{V_A$ (front hook), V_{BL} (left rear hook), V_{BR} (right rear hook)$\}$ (in lb) and the tangential tensile stresses $\{\sigma_1, \sigma_2, \sigma_3,\}$ (in ksi) at the respective hook critical stress points {1, 2, 3} were previously established as (ref. 2)

Front hook:

$$\sigma_1 = 7.3522 \times 10^{-3} V_A \tag{1}$$

Left rear hook:

$$\sigma_2 = 5.8442 \times 10^{-3} V_{BL} \tag{2}$$

Right rear hook:

$$\sigma_3 = 5.8442 \times 10^{-3} V_{BR} \tag{3}$$

During the flight tests, the loading spectra of $\{V_A, V_{BL}, V_{BR}\}$ are obtained from the outputs of strain gages attached in the vicinity of the critical stress points of the hooks. The random cycling spectra of the critical point stress $\{\sigma_1, \sigma_2, \sigma_3\}$ are then calculated from equations (1) through (3) respectively.

Figure 5 shows the random loading spectra for the three hooks during the takeoff and ascent of the B-52B carrying the SRB/DTV. Note that the magnitude of hook loading is more severe during the takeoff run than during airborne cruising. Figure 6 shows similar data during the landing of the B-52B carrying the SRB/DTV after an aborted flight test. Based on the data in figure 6, the peak hook loads at the moment of touchdown are listed in table 1 below.

Table 1. Peak touchdown hook loads; SRB/DTV.

Proof hook load, lb	Touchdown hook load, lb	Fraction of proof hook load
$V_A^p = 36{,}520$	$V_A = 25{,}600$	$f = 0.7$
$V_{BL}^p = 44{,}110$	$V_{BL} = 29{,}000$	$f = 0.6574$
$V_{BR}^p = 44{,}230$	$V_{BR} = 25{,}500$	$f = 0.5765$

From figures 5 and 6, it is seen that landing consumed far more fatigue life than the takeoff run.

Figures 7–12 show portions of the random stress cycling spectra of $\{\sigma_1, \sigma_2, \sigma_3\}$ of the front and rear hooks carrying the SRB/DTV (figs. 7, 9, and 11), and the corresponding fatigue crack growth curves (figs. 8, 10, and 12). The fatigue crack growth curves shown in figures 8, 10, and 12 were calculated using the half-cycle theory to estimate the damage done by each half cycle of the random stress cycle spectra shown in figures 7, 9, and 11 (refs. 3, 4), the only data available. Note that taxiing and takeoff consumed a great deal of hook service life because of higher crack growth rate due to high amplitude stress cycling because of ground surface effect. The crack growth rate then slowed during cruise because of the smooth air and the absence of ground surface effect.

CONVENTIONAL AGING THEORY

For each airborne structural component (e.g., B-52B pylon hook), let a_c^p be the initial fictitious crack size at the critical stress point associated with the static proof load test, and let a_c^o be the corresponding operational crack size associated with the peak operational load (a fraction of the proof load), then $\{a_c^p, a_c^o\}$ can be calculated respectively from the following crack tip equations based on fracture mechanics:

$$a_c^p = \frac{Q}{\pi}\left(\frac{K_{I_C}}{AM_K\sigma^*}\right)^2 \tag{4}$$

$$a_c^o = \frac{Q}{\pi}\left(\frac{K_{I_C}}{AM_K f\sigma^*}\right)^2 \quad ; \quad f < 1 \tag{5}$$

where K_{I_C} is the critical stress intensity factor, σ^* is the value of $\{\sigma_1^*, \sigma_2^*, \sigma_3^*\}$ at the respective critical stress point calculated respectively from equations (1)–(3) using the respective hook proof load values $\{V_A^p, V_{BL}^p, V_{BR}^p\}$; $f\sigma^*$ ($f < 1$) is the operational stress at the critical stress point; A is the crack location parameter ($A = 1$ for through-thickness cracks, $A = 1.12$ for both surface and edge cracks); and M_K is the flaw magnification factor ($M_K = 1$ for very shallow surface cracks, $M_K = 1.6$ when the crack depth approaches the back surface). Finally, Q is the surface flaw shape and plasticity factor for an elliptic surface crack (length $2c$, depth a) (fig. 14, ref. 4) and is described as

$$Q = \left[E(k)\right]^2 - 0.212\left(\frac{\sigma^*}{\sigma_Y}\right)^2 \tag{6}$$

where σ_Y is the yield stress, and $E(k)$ is the complete elliptic function of the second kind defined as

$$E(k) = \int_0^{\frac{\pi}{2}} \sqrt{1 - k^2\sin^2\phi}\; d\phi \tag{7}$$

Because $f < 1$, the size of a_c^o is larger than that of a_c^p (equations (4), (5)), the crack size differential $(a_c^o - a_c^p)$ will be the limit of available crack growth for setting the number of safe flights.

If Δa_1 is the amount of fictitious crack growth from the size a_c^p during the first test flight, then the conventional age equation for estimating the available number of flights F_1 for a particular airborne critical structural component is given by

$$F_1 = \frac{a_c^o - a_c^p}{\Delta a_1} \tag{8}$$

Equation (8) assumes that the amount of crack growth per flight remains constant, and therefore, after each test flight, the number of safe flights will decrease linearly by just one flight. This assumption is highly inaccurate because the crack growth is progressive. As such, equation (8) is nonconservative and overpredicts the number of safe flights. Thus, for safe flight tests, more conservative and accurate aging theories are needed.

CRACK GROWTH CALCULATIONS

For constant-amplitude stress cycling, the fatigue crack growth is described by the following well-known Walker crack growth rate equation:

$$\frac{da}{dN} = C(K_{\max})^m(1-R)^n = C(\Delta K)^m(1-R)^{n-m} \tag{9}$$

where, C, m, n are material constants, $K_{\max}$ is the maximum stress intensity factor, ΔK is the stress intensity amplitude, and R is the stress ratio given respectively by

$$K_{\max} = AM_k\sigma_{\max}\sqrt{\frac{\pi a}{Q}} \tag{10}$$

$$\Delta K = AM_k(\sigma_{\max} - \sigma_{\min})\sqrt{\frac{\pi a}{Q}} \tag{11}$$

$$R = \frac{\sigma_{\min}}{\sigma_{\max}} \tag{12}$$

where $\sigma_{\max}$ and $\sigma_{\min}$ are respectively the maximum and the minimum stresses of constant amplitude stress cycles.

For the random stress cycling, the half-cycle theory (refs. 3–7) may be used for the fatigue crack calculations. The half-cycle theory assumes that Walker crack growth equations (9)–(12) are valid to describe the damage done by each half cycle of the random loading spectrum. Under such an assumption, the amount of crack growth δa_i caused by the i-th (i = 1, 2, 3, . . .) half cycle of the random loading spectrum may be written from equation (9) by setting $da = \delta a_i$ and $dN = 1/2$. Namely:

$$\delta a_i = \frac{1}{2}C\left[(K_{\max})_i\right]^m(1-R_i)^n = \frac{1}{2}C(\Delta K_i)^m(1-R_i)^{n-m} \tag{13}$$

with

$$(K_{\max})_i = AM_k(\sigma_{\max})_i\sqrt{\frac{\pi a_{i-1}}{Q}} \tag{14}$$

$$(\Delta K)_i = AM_k\left[(\sigma_{\max})_i - (\sigma_{\min})_i\right]\sqrt{\frac{\pi a_{i-1}}{Q}} \tag{15}$$

$$R_i = \frac{(\sigma_{\min})_i}{(\sigma_{\max})_i} \tag{16}$$

where the subscript i (i = 1, 2, 3, . . .) is associated with the i-th half cycle, and a_{i-1} is the crack size at the end of the (i – 1)-th half cycle.

If N_l is the total number of random stress cycles induced by the l-th (l = 1, 2, 3, . . .) flight, then the amount of crack growth Δa_l caused by the l-th flight may be calculated from

$$\Delta a_l = \sum_{i=1}^{2N_l} \delta a_i \tag{17}$$

In equation (17), the calculation of the right-hand side can be carried out through the use of special computer programs which sweep through all of the random stress-cycle data to pick up the values of $\{(\sigma_{\max})_i, (\sigma_{\min})_i\}$ and calculate δa_i [equations (13)–(16)] for each half cycle, and then sum δa_i over $2N_l$ half cycles (not N_l) to obtain the value of Δa_l.

It must be mentioned that the predictions of fatigue life by the half-cycle theory compare well with the experimental fatigue data (ref. 3). Figure 13 illustrates the method of summing up the crack growth increments caused by the random stress cycling when the half-cycle theory is used (refs. 5–7).

EQUIVALENT-CONSTANT-AMPLITUDE AGING THEORIES

The purpose of establishing the equivalent-constant-amplitude aging theories is to use the first-flight data to predict the number of future safe flights when the crack growth data for subsequent flights are not available. The approaches of the new aging theories are described below.

First, the random loading spectrum obtained from the first-flight data is represented with an “equivalent-constant-amplitude loading spectrum”; then the Walker crack growth equation (9) is used to formulate the new aging theories for the calculations of the number of future safe flights. The equivalent-constant-amplitude loading spectrum is assumed to cause the same damage effect as the actual random loading spectrum based on the following assumptions:

1. The equivalent-constant-amplitude-loading spectrum induces the same amount of crack growth as Δa_l (l = 1, 2, 3, . . .) caused by the random loading spectrum of each flight.

2. The equivalent-constant-amplitude loading spectrum has the same number of stress cycles N_l (l = 1, 2, 3, . . .) as the random loading spectrum of each flight.

3. The values of $\{\sigma_{\max}, R, N_l\}$ for the equivalent-constant-amplitude loading spectra remain the same for all flights.

The equivalent-constant-amplitude aging theories will be formulated by the following two approaches: the "discrete" aging theory and the "closed-form" aging theory.

Discrete Aging Theory

For the discrete aging theory using an "equivalent-constant amplitude loading spectrum," the Walker crack growth rate equation (9) is written in finite-difference form with each flight duration as a finite-difference interval. Then, the crack growth Δa_l of the l-th flight is expressed in terms of the crack growth Δa_1 of the first flight in the formulation of the discrete aging theory.

1. Crack Growth

Writing $K_{\max}$ [equation (10)] for the ($l-1$)-th flight in the following form:

$$K_{\max} = AM_k\sigma_{\max}\sqrt{\frac{\pi a_{l-1}}{Q}} \tag{18}$$

where a_{l-1} is the crack size at the end of the (l – 1)-th flight. Then the Walker equation (9) may be written in the following finite-difference form to relate the number of stress cycles N_l to the corresponding crack growth Δa_l for the l-th flight (refs. 5–7) as

$$\Delta a_l = C\left(AM_k\sigma_{\max}\sqrt{\frac{\pi}{Q}}\right)^m (1-R)^n\,(a_{l-1})^{\frac{m}{2}} N_l \tag{19}$$

For the first flight, $a_{l-1} = a_{1-1} = a_c^p$, and equation (19) takes on the following form:

$$\Delta a_1 = C\left(AM_k\sigma_{\max}\sqrt{\frac{\pi}{Q}}\right)^m (1-R)^n (a_c^p)^{\frac{m}{2}} N_1 \tag{20}$$

Because the values of $\{\sigma_{\max}, R, N_1\}$ are assumed to remain the same for all flights, Δa_l is proportional to $(a_{l-1})^{\frac{m}{2}}$ only, and equation (19) written for the l-th flight may be divided by equation (20) written for the first flight to relate Δa_l of the l-th flight to Δa_1 of the first flight. Namely,

$$\frac{\Delta a_1}{\Delta a_1} = \left(\frac{a_c^p}{a_c^p}\right)^{\frac{m}{2}} = 1 \tag{21}$$

$$\frac{\Delta a_2}{\Delta a_1} = \left(\frac{a_1}{a_c^p}\right)^{\frac{m}{2}} = \left(1 + \frac{\Delta a_1}{a_c^p}\right)^{\frac{m}{2}} \tag{22}$$

$$\frac{\Delta a_3}{\Delta a_1} = \left(\frac{a_2}{a_c^p}\right)^{\frac{m}{2}} = \left(1 + \frac{\Delta a_1 + \Delta a_2}{a_c^p}\right)^{\frac{m}{2}} \tag{23}$$

$$\frac{\Delta a_4}{\Delta a_1} = \left(\frac{a_3}{a_c^p}\right)^{\frac{m}{2}} = \left(1 + \frac{\Delta a_1 + \Delta a_2 + \Delta a_3}{a_c^p}\right)^{\frac{m}{2}} \tag{24}$$

. . . . . .

$$\frac{\Delta a_l}{\Delta a_1} = \left(\frac{a_{l-1}}{a_c^p}\right)^{\frac{m}{2}} = \left(1 + \frac{\Delta a_1 + \Delta a_2 + \Delta a_3 + \ldots + \Delta a_{l-1}}{a_c^p}\right)^{\frac{m}{2}} \tag{25}$$

. . . . . .

$$\frac{\Delta a_{F^*}}{\Delta a_1} = \left(\frac{a_{F^*-1}}{a_c^p}\right)^{\frac{m}{2}} = \left(1 + \frac{\Delta a_1 + \Delta a_2 + \Delta a_3 + \ldots + \Delta a_l + \ldots + \Delta a_{F^*-1}}{a_c^p}\right)^{\frac{m}{2}} \tag{26}$$

It is seen that the crack growth Δa_l for the *l*-th flight is expressed in terms of the crack growth of all previous flights $(\Delta a_1, \Delta a_2, \Delta a_3, \Delta a_4, \ldots, \Delta a_{l-1})$, and that the amount of crack growth is progressive, meaning the amount of crack growth Δa_l will continue to increase with the increasing number of flights (i.e., $\Delta a_1 < \Delta a_2 < \Delta a_3 < \ldots < \Delta a_l < \ldots$).

In light of equations (21)–(26), if the crack growth Δa_1 of the first flight is known (i.e., calculated from equation (17) from the first-flight data), then the crack growths $(\Delta a_2, \Delta a_3, \Delta a_4, \ldots, \Delta a_l, \ldots, \Delta a_{F^*})$ for all subsequent flights can be calculated. This is the essence of the discrete aging theory.

For mathematical simplification, the right-hand sides of equations (21)–(26) have been expanded to the first- and second-order terms. The Ko first-order (ref. 5) and Ko second-order (refs. 6, 7) explicit aging equations were developed for the calculations of the number of safe flights $\{\bar{F}_1, \tilde{F}_1\}$. Those explicit aging equations based on the Ko first- and Ko second-order aging theories are taken from references 5–7 and are referred to in the appendix.

2. Number of Safe Flights

When the crack growth summation $(\Delta a_1 + \Delta a_2 + \Delta a_3 + \ . \ . \ . \ + \Delta a_{F^*-1} + \Delta a_{F^*})$ reaches the size of the available crack differential $(a_c^o - a_c^p)$, one can write

$$\underbrace{\Delta a_1 + \Delta a_2 + \Delta a_3 + \ . \ . \ . \ + \Delta a_{F^*-1} + \Delta a_{F^*}}_{|\text{<----------}F^*\text{ terms----------}>|} = a_c^o - a_c^p = F_1 \times \Delta a_1 \tag{27}$$

Equation (27) is an implicit aging equation based on the discrete aging theory for finding the number of safe flights F^*. By substituting equations (21)–(26) into equation (27) with Δa_1 of the first flight calculated from equation (17), the number of safe flights F^* can be calculated.

In the computational process to find the value of F^* from equation (27), the number of terms of summation of Δa_l on the left-hand side was successively increased step-by-step until the value of summation of the left-hand side approached the value of $(a_c^o - a_c^p)$ on the right-hand side.

Closed-Form Aging Theory

For the closed-form aging theory based on the "equivalent-constant-amplitude loading spectrum", the aging equation will be formulated through the integration of the Walker crack-growth-rate equation (9). The closed-form aging theory will then be used to check the accuracy of the discrete aging theory.

1. Crack Growth

To formulate the closed-form aging theory, equation (10) is substituted into the Walker crack-growth-rate equation (9) to yield the following form:

$$\frac{da}{dN} = C\left[AM_K\sigma_{\max}\sqrt{\frac{\pi}{Q}}\right]^m (1-R)^n (a)^{\frac{m}{2}} \tag{28}$$

which, after rearranging, becomes

$$\left(\frac{1}{a}\right)^{\frac{m}{2}} da = C\left[AM_K\sigma_{\max}\sqrt{\frac{\pi}{Q}}\right]^m (1-R)^n \, dN \tag{29}$$

Because the values of $\{\sigma_{\max}, R\}$ are assumed to remain unchanged for all flights, equation (29) may be easily integrated from a_c^p to arbitrary crack size a for the left-hand side, and from 0 to the corresponding number of stress cycles N for the right-hand side as

$$\left(a_c^p\right)^{1-\frac{m}{2}} - \left(a\right)^{1-\frac{m}{2}} = C\left(\frac{m}{2}-1\right)\left(AM_K\sigma_{\max}\sqrt{\frac{\pi}{Q}}\right)^m (1-R)^n N \tag{30}$$

which may be re-written in alternative form as

$$a = \left[\left(a_c^p\right)^{1-\frac{m}{2}} - C\left(\frac{m}{2}-1\right)\left(AM_K\sigma_{\max}\sqrt{\frac{\pi}{Q}}\right)^m (1-R)^n N\right]^{\frac{2}{2-m}} \tag{31}$$

Equation (31) is to be used to plot the crack size a as a function of number of stress cycles N.

Also, integration of equation (29) over each flight interval with N_l number of stress cycles, yields the following "powered" crack-growth equation for each flight:

First flight:

$$\left(a_c^p\right)^{1-\frac{m}{2}} - \left(a_1\right)^{1-\frac{m}{2}} = C\left(\frac{m}{2}-1\right)\left[AM_K\sigma_{\max}\sqrt{\frac{\pi}{Q}}\right]^m (1-R)^n N_1 \tag{32}$$

Second flight:

$$\left(a_1\right)^{1-\frac{m}{2}} - \left(a_2\right)^{1-\frac{m}{2}} = C\left(\frac{m}{2}-1\right)\left(AM_K\sigma_{\max}\sqrt{\frac{\pi}{Q}}\right)^m (1-R)^n N_2 \tag{33}$$

. . . . . .

l-th flight

$$\left(a_{l-1}\right)^{1-\frac{m}{2}} - \left(a_l\right)^{1-\frac{m}{2}} = C\left(\frac{m}{2}-1\right)\left(AM_K\sigma_{\max}\sqrt{\frac{\pi}{Q}}\right)^m (1-R)^n N_l \tag{34}$$

. . . . . .

F_1^*-th flight (Final flight)

$$\left(a_{F_1^*-1}\right)^{1-\frac{m}{2}} - \left(a_{F_1^*}\right)^{1-\frac{m}{2}} = C\left(\frac{m}{2}-1\right)\left(AM_K\sigma_{\max}\sqrt{\frac{\pi}{Q}}\right)^m (1-R)^n N_{F_1^*} \;;\; a_{F_1^*} = a_c^o \tag{35}$$

The earlier assumption that the loading spectra of all flights have the same number of stress cycles:

$$N_1 = N_2 = N_3 = \ldots = N_l = \ldots = N_{F_1^*} \tag{36}$$

gives the following "powered" crack-growth relationships between all flights:

$$\left(a_c^p\right)^{1-\frac{m}{2}} - \left(a_1\right)^{1-\frac{m}{2}} = \left(a_1\right)^{1-\frac{m}{2}} - \left(a_2\right)^{1-\frac{m}{2}} = \ldots\ldots \tag{37}$$

$$\ldots\ldots = \left(a_{l-1}\right)^{1-\frac{m}{2}} - \left(a_l\right)^{1-\frac{m}{2}} = \ldots\ldots = \left(a_{F_1^*-1}\right)^{1-\frac{m}{2}} - \left(a_{F_1^*}\right)^{1-\frac{m}{2}}$$

2. Number of Safe Flights

By adding all the crack-growth equations (32)–(35) from flight $l = 1$ to $l = F_1^*$, and noting that $a_{F_1^*} = a_c^o$, there results:

$$\left(a_c^p\right)^{1-\frac{m}{2}} - \left(a_c^o\right)^{1-\frac{m}{2}} \tag{38}$$

$$= C\left(\frac{m}{2}-1\right)\left(AM_K\sigma_{\max}\sqrt{\frac{\pi}{Q}}\right)^m (1-R)^n \left(N_1 + N_2 + \ldots + N_l + \ldots + N_{F_1^*}\right)$$

Dividing equation (38) by equation (32) results in an explicit aging equation for the calculation of the number of safe flights F_1^*:

$$\frac{\overbrace{\left(N_1 + N_2 + N_3 + \ldots + N_l + \ldots + N_{F_1^*}\right)}^{|\text{<----------}F^*\text{ terms----------}>|}}{N_1} = \frac{\left(a_c^p\right)^{1-\frac{m}{2}} - \left(a_c^o\right)^{1-\frac{m}{2}}}{\left(a_c^p\right)^{1-\frac{m}{2}} - \left(a_1\right)^{1-\frac{m}{2}}} \tag{39}$$

which, in light of the assumed condition (36), becomes

$$\frac{F_1^* \times N_1}{N_1} = F_1^* = \frac{\left(a_c^p\right)^{1-\frac{m}{2}} - \left(a_c^o\right)^{1-\frac{m}{2}}}{\left(a_c^p\right)^{1-\frac{m}{2}} - \left(a_1\right)^{1-\frac{m}{2}}} \tag{40}$$

which is the aging equation for calculating the number of safe flights F_1^* based on the closed-form aging theory.

Alternatively, writing equation (30) for the flight age limit (i.e., $a = a_c^o$, $N = N_{total}$), we have

$$\left(a_c^p\right)^{1-\frac{m}{2}} - \left(a_c^o\right)^{1-\frac{m}{2}} = C\left(\frac{m}{2}-1\right)\left(AM_K\sigma_{\max}\sqrt{\frac{\pi}{Q}}\right)^m (1-R)^n N_{total} \tag{41}$$

Because of the assumption $N_{total} = F_1^* \times N_1$, division of equation (41) by equation (32) will yield the aging equation identical to equation (40).

It must be mentioned that for the value of crack size $a_1 = a_c^p + \Delta a_1$ $(l = 1)$ for the first flight, Δa_1 is to be calculated from equation (17) using the half-cycle theory as mentioned earlier.

EQUIVALENT STRESS AMPLITUDES

In the previous formulations of the equivalent-constant-amplitude aging theories, $\{\sigma_{\max}, R, N_l\}$ were eliminated through division processes and, therefore did not appear in the final aging equations. Thus, there is no need to know the actual magnitudes of $\{\sigma_{\max}, R, N_l\}$.

In fact, each random loading spectrum could be represented by a multiple number of equivalent-constant-amplitude loading spectra based on the selections of the values of $\{\sigma_{\max}, R, N_l\}$.

For the purpose of visualization, we will calculate the values of $\{\sigma_{\max}, \sigma_{\min}, R\}$, and plot against the random loading spectra flight data for comparisons.

To determine the maximum stress $\sigma_{\max}$ and the mean stress σ_s of the equivalent-constant-amplitude loading spectrum, equation (30) may be rewritten in the following form:

$$(\sigma_{\max})^m (1-R)^n = \frac{2}{C(m-2)}\left(\frac{1}{AM_K}\sqrt{\frac{Q}{\pi}}\right)^m \frac{\left(a_c^p\right)^{1-\frac{m}{2}} - \left(a_1\right)^{1-\frac{m}{2}}}{N_1} \tag{42}$$

For the equivalent-constant-amplitude load spectrum, the following relationship holds:

$$\sigma_{\min} = 2\sigma_s - \sigma_{\max} \tag{43}$$

$$R = \frac{\sigma_{\min}}{\sigma_{\max}} = \frac{2\sigma_s}{\sigma_{\max}} - 1 \tag{44}$$

Substitution of relationships (43) and (44) into the left-hand side of equation (42) yields:

$$(\sigma_{\max})^m\left(1-\frac{\sigma_s}{\sigma_{\max}}\right)^n = \frac{(2)^{1-n}}{C(m-2)}\left(\frac{1}{AM_k}\sqrt{\frac{Q}{\pi}}\right)^m \frac{\left(a_c^p\right)^{1-\frac{m}{2}}-\left(a_1\right)^{1-\frac{m}{2}}}{N_1} \tag{45}$$

In equation (45), the right-hand side is known, and the left-hand side has two unknowns: $\sigma_{\max}$ and σ_s. Thus, there are multiple combinations of $\sigma_{\max}$ and σ_s for finding the equivalent-constant-amplitude load spectrum. The most practical way is to choose the value of the mean stress σ_s of the random loading spectrum by inspection, and then calculate the equivalent maximum stress $\sigma_{\max}$ from equation (45).

NUMERICAL EXAMPLE

The numerical example is to demonstrate how to calculate the number of safe flights for a flight test program. The example chosen is the NASA B-52B carrier aircraft pylon hooks (one front hook, two rear hooks) (figs.1, 2) carrying the Pegasus winged three-stage solid rocket (44,629 lb) up to high altitude (approximately 40,000 ft) for air-launching, firing and sending the payload into orbit.

Material Properties

The material properties of the B-52B pylon front and rear hooks are listed in table 2.

Table 2. Material properties of B-52B pylon hooks.

Part name	Material	σ_U ksi	σ_Y ksi	τ_U ksi	K_{I_C} ksi$\sqrt{\text{in.}}$	C $\frac{\text{in.}}{cycle}(\text{ksi}\sqrt{\text{in.}})^{-m}$	m	n
Front hook	Inconel 718*	175	145	135	125	9.220×10^{-12}	3.60	2.16
Rear hooks	AMAX MP35N†	250	235	141	124	2.944×10^{-11}	3.24	1.69

* Inco Alloys International, Inc., Huntington, West Virginia.
† H. C. Starck, Inc., Cleveland, Ohio.

Input Crack Data

The fictitious surface crack at the critical stress point of each hook is assumed to be semicircular in shape ($c = a$, fig. 14). This is based on the observations of the past failed B-52B pylon two rear hooks. The crack propagation initiation sites of the failed hooks were almost semi-circular surface cracks of depths a = 0.031 in. and a = 0.038 in. respectively for the inboard and outboard hooks (ref. 2). Note from figure 14 that the semicircular surface crack has the relatively high value of Q. Other crack parameters used were: A = 1.12 for the surface crack, and M_K = 1.0 for the high (hook depth) to (crack depth) ratios.

Before the test flights, the approximate number of safe flights must be estimated. Because the actual random loading spectrum for each hook is not available for the calculation of the amount of crack growth Δa_1 for the first flight, the value of $\frac{\Delta a_1}{a_c^p}$ for each hook may be based on the earlier test data of SRB/DTV because of the weight proximity of the two vehicles. The SRB/DTV (49,000 lb) is only 8.92 percent heavier than the Pegasus winged rocket (44,692 lb).

The initial crack size a_c^p, the operational crack size a_c^o, and the crack growth $\frac{\Delta a_1}{a_c^p}$ used in the aging analysis for the case of the Pegasus winged rocket are listed in table 3.

Table 3. Proof and operational crack sizes for B-52B pylon hooks carrying Pegasus winged rocket (44,692 lb).

Hook name	Hook proof load, lb	a_c^p, in. (f = 1.0)	a_c^o in. (f = 0.6)	$\frac{\Delta a_1}{a_c^p}$
Front, V_A	36,500	0.1247	0.3465	0.01814
Rear left, V_{BL}	57,819	0.0774	0.2151	0.00761
Rear left, V_{BR}	57,819	0.0774	0.2151	0.00989

In table 3, the value of initial crack size a_c^p and the operational crack size a_c^o are calculated respectively from equations (4) and (5). The value of a_c^o was calculated based on the assumption that operational peak stress is 60 percent of the proof stress (i.e., f = 0.6). This f value is slightly higher (more conservative) than the f values in the SRB/DTV case, for which the f value for the front hook is f = 0.5450, for the left rear hook, f = 0.5946, and for the rear right hook, f = 0.5986 (refs. 4, 5).

Note that in table 3, the crack growth $\frac{\Delta a_1}{a_c^p}$ of the right rear hook is 1.3 times larger than $\frac{\Delta a_1}{a_c^p}$ of the rear left hook. This is based on SRB/DTV flight data which show that the crack growth rate for the right rear hook is 1.3 times larger than that of the left rear hook as a result of the combined aerodynamic, inertial, and static loads.

Equivalent-Constant-Stress Amplitudes

The typical duration of a B-52B air-launch test flight is about 50 minutes (in the SRB/DTV case), and the random loading spectrum has 4 cycles per second. Therefore, the number of stress cycles is N_1 = 12,000 (= 50 × 60 × 4) cycles per flight. This value will be used in generating the equivalent-constant-amplitude loading spectrum. Table 4 shows the calculated value of $\{\sigma_{\max}, \sigma_{\min}, R\}$ associated with the equivalent-constant-amplitude load spectrum for given N_1, $\Delta a_1 / a_c^p$ and σ_s.

Table 4. Stress values for the equivalent-constant-amplitude loading spectra; N_1 = 12,000 cycles: $\Delta a_1 / a_c^p$ and σ_s given.

Hook	$\frac{\Delta a_1}{a_c^p}$ (Given)	σ_s, ksi (Given)	$\sigma_{\max}$, ksi (f)	$\sigma_{\min}$, ksi	R
Front (V_A)	0.01814	108.000	115.406 (0.43)	100.594	0.8717
Rear left (V_{BL})	0.00761	127.000	130.157 (0.50)	123.843	0.9515
Rear right (V_{BR})	0.00989	132.500	136.051 (0.53)	128.949	0.9478

Figures 15–17 compare the actual random loading spectra (using available data of SRB/DTV) and the associated equivalent-constant-stress amplitude stress cycles for the three hooks based on the data listed in table 3. Notice that the f values for the equivalent-constant-stress amplitude stress cycles to cause the same amount of damage as the random loading spectra are only in the range of f = 0.43–0.53 (much less than f = 0.6).

Number of Safe Flights

Figures 18–20 show normalized crack sizes $(\Delta a_l / \Delta a_1)$ plotted as functions of the number of the flight (l) for the front and the rear hooks based on the different aging theories. The terminal point of each crack growth curve gives the predicted number of flights. Notice that the conventional aging theory gives horizontal lines (figs. 18–20) because of the assumption, $\Delta a_l = \Delta a_1$. As the aging theory is improved, the slopes of the crack growth curves become steeper and the predicted number of flights decreases. The crack growth curves based on the discrete aging theory and the closed-form aging theory are practically coincidental. The two theories predicted identical and the lowest number of flights.

Figure 21 shows the crack growth curves in the $a - N$ space for the front and rear hooks based on the closed-form aging theory [equation (31)]. For each hook, the intersection of the crack growth curve and the corresponding operational crack limit line ($a = a_c^o$ horizontal line) will give the total number of available stress cycles. After dividing the total number of cycles by 12,000 cycles per flight, one obtains the number of remaining flights F_1^* = 39, F_1^* = 100, F_1^* = 77 flights respectively for the front hook, rear left hook, and rear right hook.

Figures 22–24, respectively, show the crack growth curves for the front and the two rear hooks in the $a - flights$ space. The crack growth curve based on the classical aging theory for each hook is a straight line because of the assumption that the amount of crack growth Δa_l for every flight remains the same. The crack growth curves based on the other aging theories are nonlinear. The intersecting points of the crack growth curves and the associated horizontal operational crack limit line ($a = a_c^o$ horizontal lines) will give the number of remaining flights $\{F_1, \bar{F}_1, \tilde{F}_1, F^*, F_1^*\}$ based on the different aging theories. The values of $\{F_1, \bar{F}_1, \tilde{F}_1, F^*, F_1^*\}$ are indicated in the figures.

Table 5 summarizes the number of remaining flights $\{F_1, \bar{F}_1, \tilde{F}_1, F^*, F_1^*\}$ predicted from different aging theories for the case of B-52B hooks carrying the Pegasus launching vehicle.

Table 5. Number of safe flights predicted from different aging theories for the case of B-52B hooks carrying the Pegasus winged rocket (44,692 lb).

Hook	F_1	(F_1/F_1^*)	$\bar{F}_1$	$(\bar{F}_1/F_1^*)$	$\tilde{F}_1$	$(\tilde{F}_1/F_1^*)$	F^*	F_1^*
Front (V_A)	98	(2.51)	53	(1.36)	45	(1.15)	39	39
Rear left (V_{BL})	234	(2.34)	130	(1.30)	110	(1.10)	100	100
Rear right (V_{BR})	180	(2.34)	100	(1.30)	85	(1.10)	77	77

In table 5, the predictions from different aging theories are also normalized by the closed-form solution F_1^* (inside the parentheses). Note that the classical aging theory predicts the number of remaining flights by more than twice that predicted by the closed-form (or finite-difference) aging theory.

CONCLUDING REMARKS

New aging theories have been developed to accurately estimate the number of safe flights for airborne structural components. The highlights are listed below.

1. The newly-developed aging theories take into account the progressive crack growth problem, and, therefore, predict far fewer safe flights of airborne critical structural components than that predicted from the conventional aging theory due to the inclusion of all the higher-order terms.

2. The new aging theories and the previous Ko first- and Ko second-order aging theories agree well at a low number of flights. However, as the number of flights increases, the two previous aging theories slightly overpredict the number of remaining flights in relation to the two newly-developed aging theories which include all the higher-order terms.

3. Both the discrete and the closed-form aging theories predict a practically identical number of safe flights.

4. The closed-form aging theory provides an explicit expression of the aging equation for the calculations of the number of safe flights.

5. The discrete aging theory allows step-by-step updating of the number of remaining safe flights for geometrical visualization of how the number of remaining safe flights are consumed.

6. The front hook has the shortest flight-test life span, and therefore is the most critical structural component in determining the limit number of flights for safe flight tests.

7. In the case of the Pegasus winged rocket, the number of available safe flights for the flight tests is 39 flights.

APPENDIX

KO FIRST-ORDER AND KO SECOND-ORDER AGING THEORIES

This appendix is based on the results presented in references 5, 6, and 7.

Under the assumption that $\{\sigma_{\max}, R, N_l\}$ remain the same for all flights, and while the value of $\dfrac{\Delta a_1 + \Delta a_2 + \Delta a_3 + \ldots}{a_c^p}$ is still small (i.e., $\dfrac{\Delta a_1 + \Delta a_2 + \Delta a_3 + \ldots}{a_c^p} << 1$) during the earlier stage of flight tests (i.e., l is not large), the crack growth $\dfrac{\Delta a_l}{\Delta a_1}$ for each flight [equations (21)–(26)] may be expanded up to second-order terms as follows (refs. 5, 6, 7):

$$\frac{\Delta a_1}{\Delta a_1} = \left(\frac{a_c^p}{a_c^p}\right)^{\frac{m}{2}} = 1 \tag{A-1}$$

$$\frac{\Delta a_2}{\Delta a_1} = \left(\frac{a_1}{a_c^p}\right)^{\frac{m}{2}} = \left(1 + \frac{\Delta a_1}{a_c^p}\right)^{\frac{m}{2}} = 1 + 1\left(\frac{m}{2}\frac{\Delta a_1}{a_c^p}\right)\left[1 - \frac{1}{2}\left(\frac{m}{2}\frac{\Delta a_1}{a_c^p}\right)\right] + 1^2\left(1 - \frac{1}{m}\right)\left(\frac{m}{2}\frac{\Delta a_1}{a_c^p}\right)^2 + \ldots\ldots\ldots \tag{A-2}$$

$$\frac{\Delta a_3}{\Delta a_1} = \left(\frac{a_2}{a_c^p}\right)^{\frac{m}{2}} = \left(1 + \frac{\Delta a_1 + \Delta a_2}{a_c^p}\right)^{\frac{m}{2}} = \left[1 + \frac{\Delta a_1}{a_c^p}\left(1 + \frac{\Delta a_2}{\Delta a_1}\right)\right]^{\frac{m}{2}} \tag{A-3}$$

$$= 1 + 2\left(\frac{m}{2}\frac{\Delta a_1}{a_c^p}\right)\left[1 - \frac{1}{2}\left(\frac{m}{2}\frac{\Delta a_1}{a_c^p}\right)\right] + 2^2\left(1 - \frac{1}{m}\right)\left(\frac{m}{2}\frac{\Delta a_1}{a_c^p}\right)^2 + \ldots\ldots\ldots$$

$$\frac{\Delta a_4}{\Delta a_1} = \left(\frac{a_3}{a_c^p}\right)^{\frac{m}{2}} = \left(1 + \frac{\Delta a_1 + \Delta a_2 + \Delta a_3}{a_c^p}\right)^{\frac{m}{2}} = \left[1 + \frac{\Delta a_1}{a_c^p}\left(1 + \frac{\Delta a_2}{\Delta a_1} + \frac{\Delta a_3}{\Delta a_1}\right)\right]^{\frac{m}{2}} \tag{A-4}$$

$$= 1 + 3\left(\frac{m}{2}\frac{\Delta a_1}{a_c^p}\right)\left[1 - \frac{1}{2}\left(\frac{m}{2}\frac{\Delta a_1}{a_c^p}\right)\right] + 3^2\left(1 - \frac{1}{m}\right)\left(\frac{m}{2}\frac{\Delta a_1}{a_c^p}\right)^2 + \ldots\ldots\ldots$$

. . . . . .

$$\frac{\Delta a_l}{\Delta a_1} = \left(\frac{a_{l-1}}{a_c^p}\right)^{\frac{m}{2}} = \left(1 + \frac{\Delta a_1 + \Delta a_2 + \Delta a_3 + \ldots + \Delta a_{l-1}}{a_c^p}\right)^{\frac{m}{2}} \tag{A-5}$$

$$= \left[1 + \frac{\Delta a_1}{a_c^p}\left(\frac{\Delta a_2}{\Delta a_1} + \frac{\Delta a_3}{\Delta a_1} + \ldots + \frac{\Delta a_{l-1}}{\Delta a_1}\right)\right]^{\frac{m}{2}}$$

$$= 1 + (l-1)\left(\frac{m}{2}\frac{\Delta a_1}{a_c^p}\right)\left[1 - \frac{1}{2}\left(\frac{m}{2}\frac{\Delta a_1}{a_c^p}\right)\right] + (l-1)^2\left(1 - \frac{1}{m}\right)\left(\frac{m}{2}\frac{\Delta a_1}{a_c^p}\right)^2 + \ldots\ldots.$$

. . . . . .

Ko First-Order Aging Theory

The first-order expansion of $\frac{\Delta a_l}{\Delta a_1}$ [equations (A-1)–(A-5)] gives the following first-order aging formula for the calculation of the remaining flights $\bar{F}_1$ (ref. 5).

$$\bar{F}_1 = \frac{2a_c^p}{m\Delta a_1}\left(\sqrt{1 + \frac{m\Delta a_1}{a_c^p}F_1} - 1\right) \tag{A-6}$$

Notice that the number of remaining flights $\bar{F}_1$ based on the Ko first-order aging theory is expressed explicitly in terms of F_1, the number of remaining flights based on the classical aging theory.

Ko Second-Order Aging Theory

By retaining up to the second-order terms of expansions in equations (A-1)–(A-5), one obtains the following Ko second-order aging equation for the calculations of remaining flights $\tilde{F}_1$ expressed explicitly in term of F_1 as follows (refs. 6, 7).

$$\tilde{F}_1 = B + D - \frac{p}{3} \tag{A-7}$$

where both B and D are functions of F_1 and are given by

$$B = \sqrt[3]{-\frac{\beta}{2} + \sqrt{\frac{\beta^2}{4} + \frac{\alpha^3}{27}}} \tag{A-8}$$

$$D = \sqrt[3]{-\frac{\beta}{2} - \sqrt{\frac{\beta^2}{4} + \frac{\alpha^3}{27}}} \tag{A-9}$$

where

$$\alpha = \frac{1}{3}(3q - p^2) \tag{A-10}$$

$$\beta = \frac{1}{27}(2p^3 - 9pq + 27r) \tag{A-11}$$

where p, q, r are the coefficients of the following cubic equation

$$\tilde{F}_1^3 + p\tilde{F}_1^2 + q\tilde{F}_1 + r = 0 \tag{A-12}$$

and are given below.

$$p = \frac{3}{2(m-1)}\left(1 - \frac{3}{2}m + 2\frac{a_c^p}{\Delta a_1}\right) \tag{A-13}$$

$$q = \frac{1}{2}\left\{1 + \frac{3}{m-1}\left[\frac{m}{2} - 2\frac{a_p^c}{\Delta a_1} + \frac{8}{m}\left(\frac{a_c^p}{\Delta a_1}\right)^2\right]\right\} \tag{A-14}$$

$$r = -\frac{12F_1}{m(m-1)}\left(\frac{a_c^p}{\Delta a_1}\right)^2 \tag{A-15}$$

Notice that F_1 (remaining safe flights based on the conventional aging theory) appears only in the expression for r in equation (A-15).

At relatively low number of flights (i.e., l is not too large), the term $\frac{\Delta a_1 + \Delta a_2 + \Delta a_3 + \ldots}{a_c^p}$ is still small $\left(\text{i.e., } \frac{\Delta a_1 + \Delta a_2 + \Delta a_3 + \ldots}{a_c^p} << 1\right)$, the Ko first- and Ko second-order aging theories could give reasonably accurate number of remaining flights. However, the two theories start to lose accuracy as the number of flight (l) increases.

REFERENCES

1. Ko, William L., *Stress Analysis of B-52 Pylon Hooks for Carrying the X-38 Drop Test Vehicle*, NASA TM-97-206218, 1997.

2. Ko, William L., and Lawrence S. Schuster, *Stress Analysis of B-52 Pylon Hooks*, NASA TM-84924, 1985.

3. Barrois, W., and E. L. Ripley, eds., *Fatigue of Aircraft Structures*, Macmillan Co.,1963.

4. Ko, William L., A. L. Carter, W. W. Totton, and J. M. Ficke, *Application of Fracture Mechanics and Half-Cycle Method to the Prediction of Fatigue Life of B-52 Aircraft Pylon Components*, NASA TM-88277, 1989.

5. Ko, William L., *Prediction of Service Life of Aircraft Structural Components Using the Half-Cycle Method*, NASA TM-86812, May 1987. Also in Folias, E.S., *International Journal of Fracture*, Vol. 39, pp. 45–62, Kluwer Academic Publishers, 1989.

6. Ko, William L., and Richard Monaghan, *Practical Theories for Service Life Prediction of Critical Aerospace Structural Components*, NASA TM-4354, 1992.

7. Ko, William L., Richard Monaghan, and Raymond H. Jackson, "Practical Theories for Service Life Prediction of Critical Aerospace Structural Components," *Structural Failure, Product Liability and Technical Insurance IV*— Proceedings of the *4th International Conference on Failure, Product Liability and Technical Insurance*, Vienna, Austria, July 6–9, 1992. Elsevier Science Publishers, July 1993.

8. Ko, William L., and Leslie Gong, *Thermostructural Analysis of Unconventional Wing Structures of a Hyper-X Hypersonic Flight Research Vehicle for the Mach 7 Mission*, NASA TP-2001-210398, 2001.

FIGURES

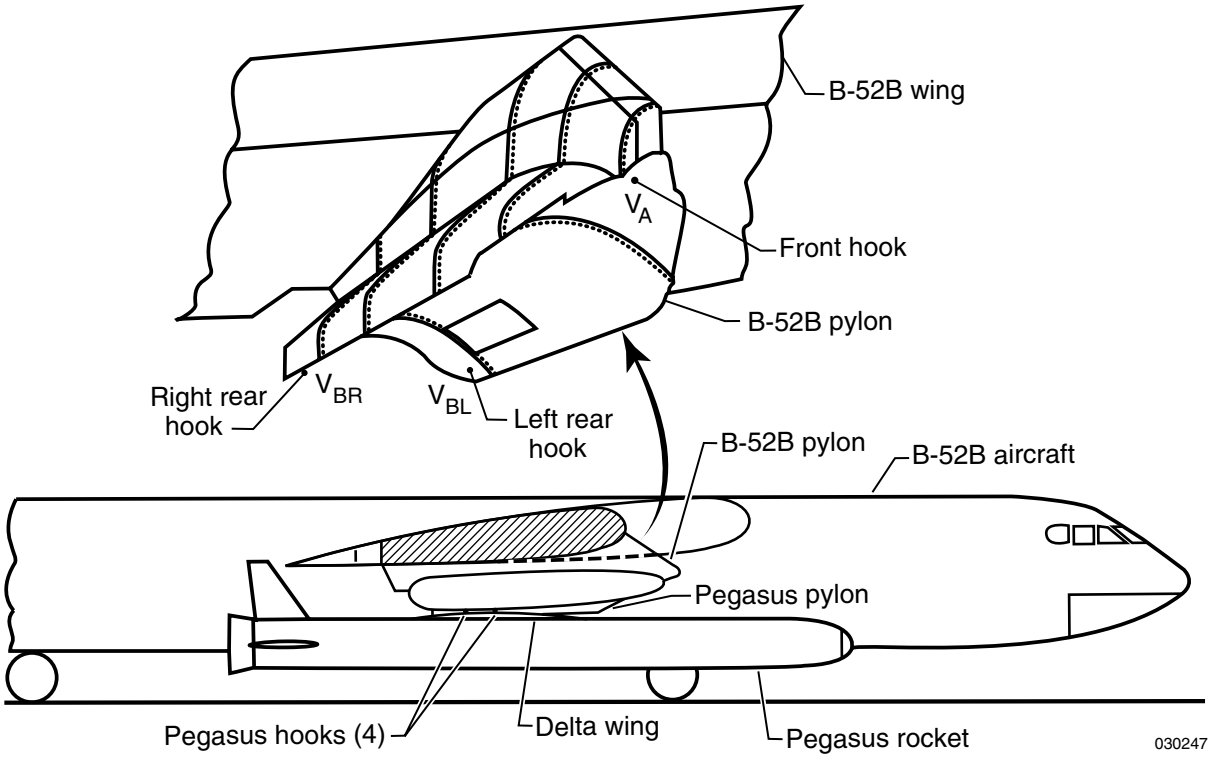

Figure 1. B-52B launching aircraft pylon carrying winged Pegasus rocket.

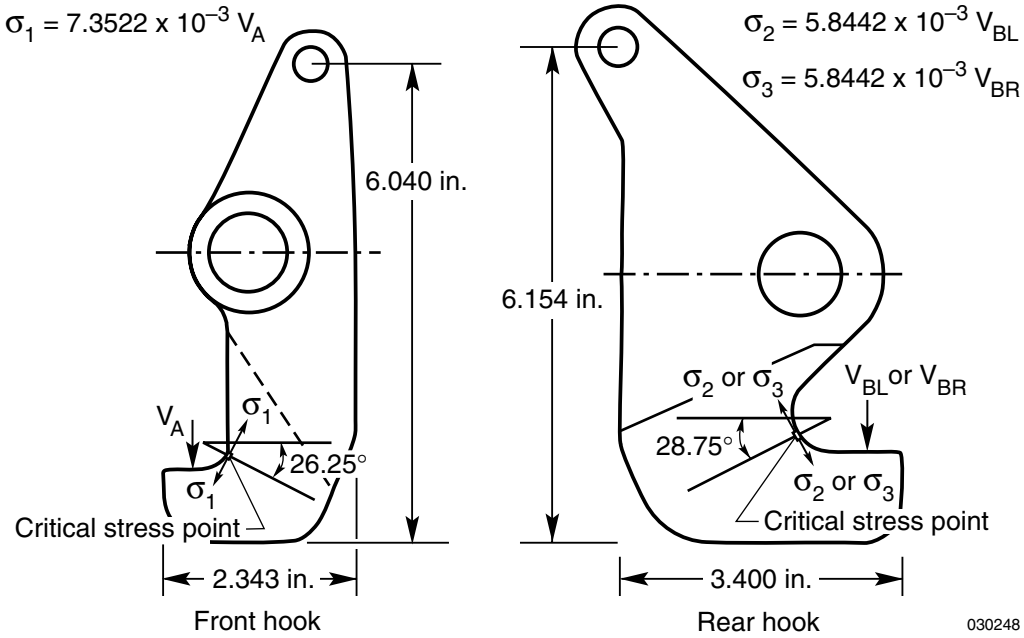

Figure 2. Critical stress points in B-52B pylon front and rear hooks.

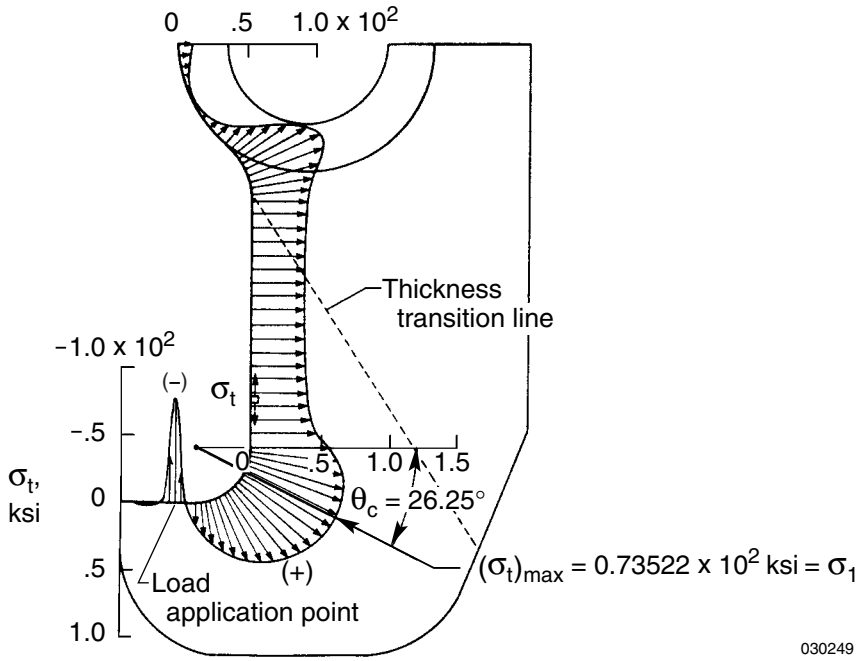

Figure 3. Distribution of tangential stress σ_t along inner boundary of front hook; $V_A = 10,000$ lb.

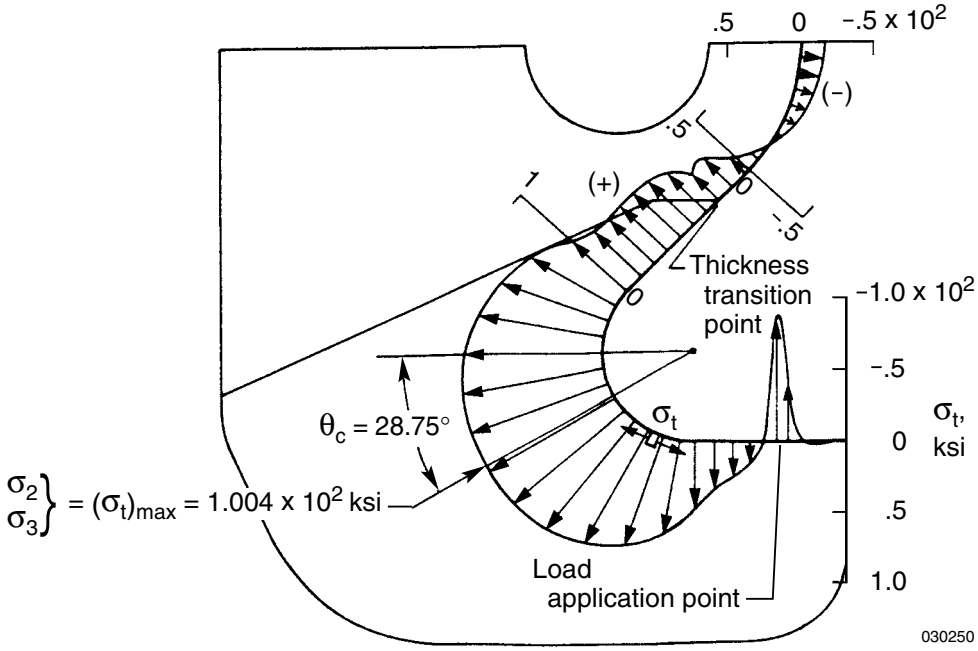

Figure 4. Distribution of tangential stress σ_t along inner boundary of rear hook; $V_{BL} = V_{BR} = 17,179.53$ lb.

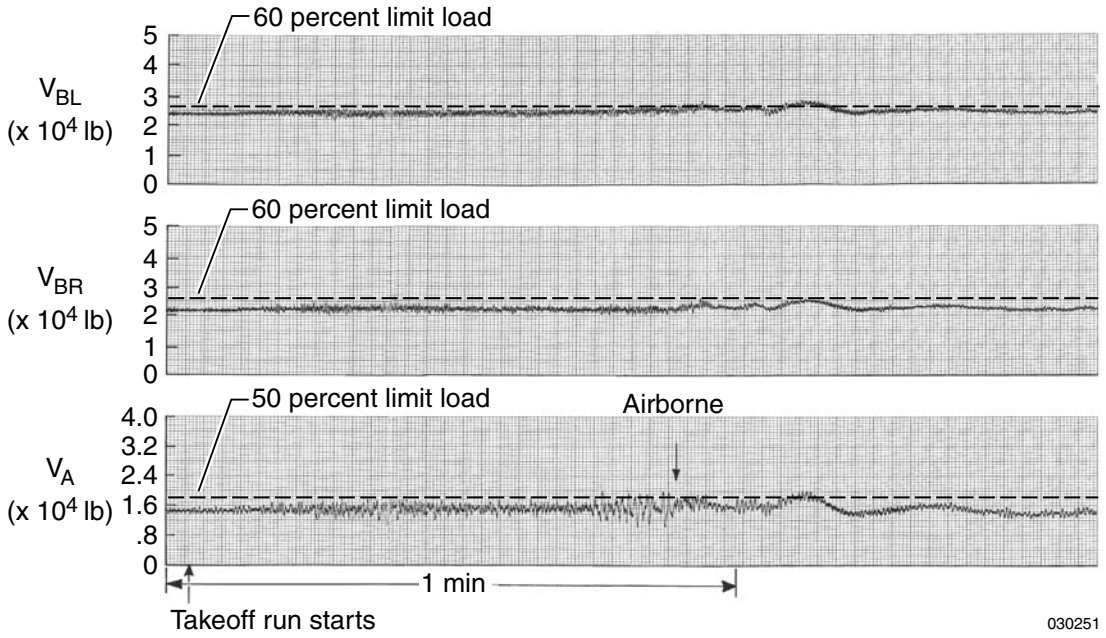

Figure 5. Random loading spectra for B-52B hooks carrying SRB/DTV (captive flight); takeoff run and airborne.

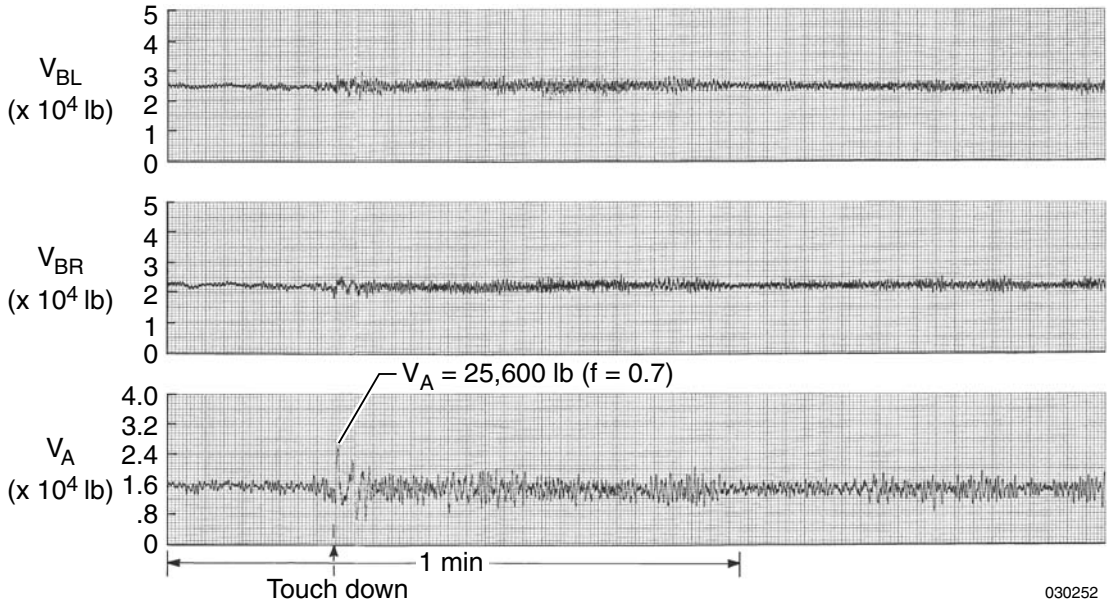

Figure 6. Random loading spectra for B-52B hooks carrying SRB/DTV (captive flight); landing and taxiing.

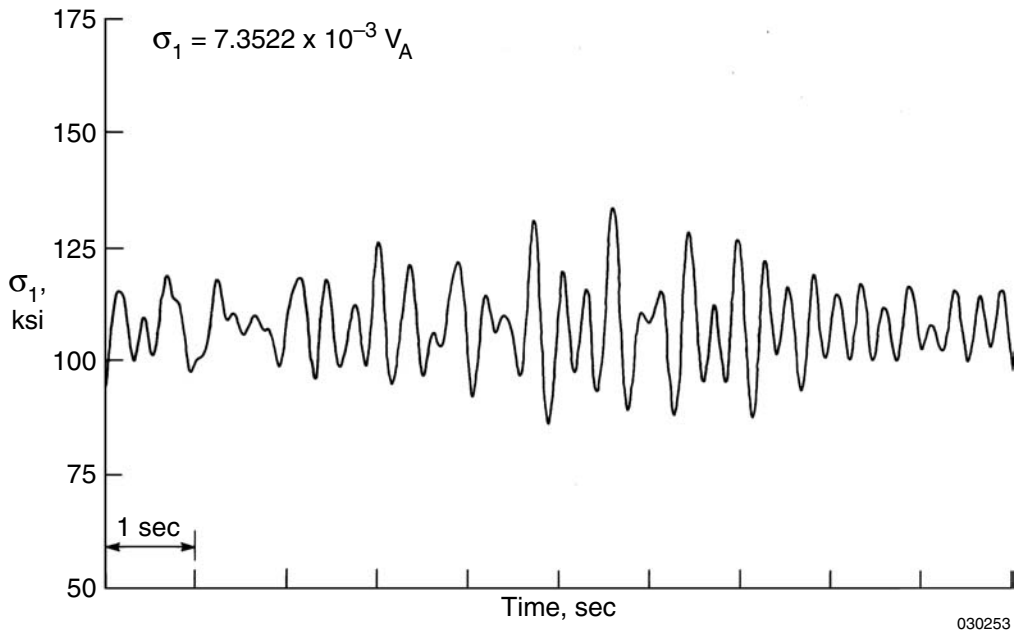

Figure 7. Typical random loading spectrum for front hook (V_A) critical stress point 1 (σ_1); B-52B carrying SRB/DTV.

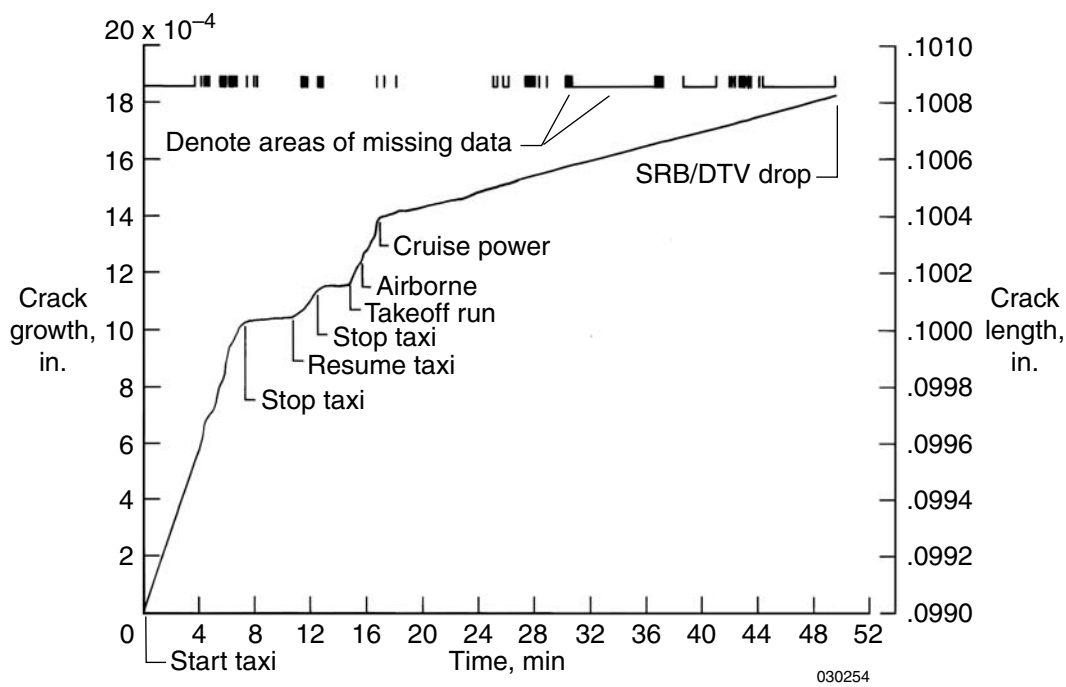

Figure 8. Crack growth curve for front hook (V_A) critical stress point 1 (σ_1); B-52B carrying SRB/DTV.

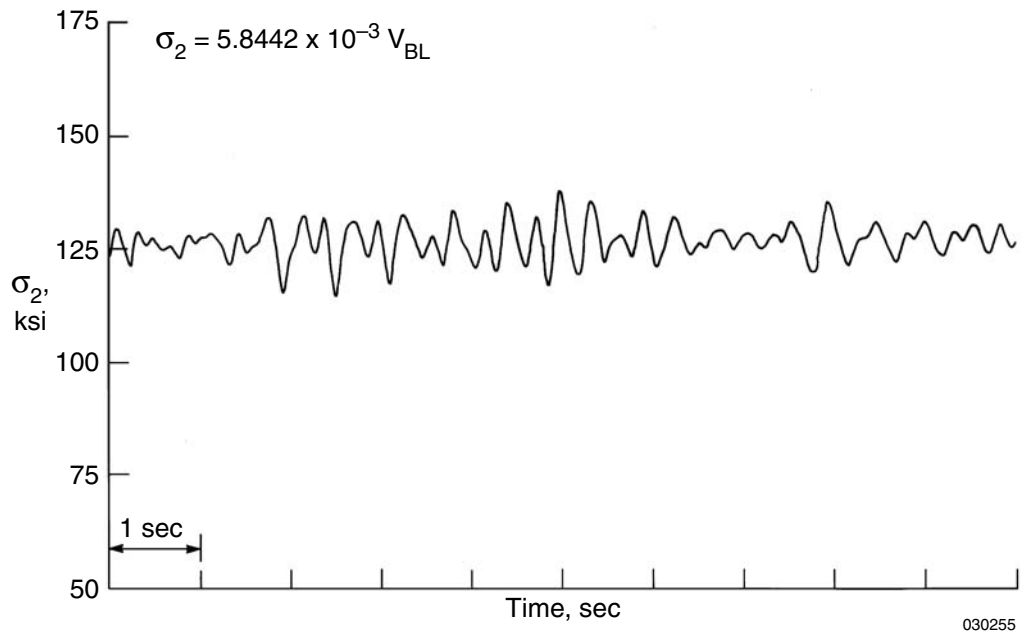

Figure 9. Typical random loading spectrum for left rear hook (V_{BL}) critical stress point 2 (σ_2); B-52B carrying SRB/DTV.

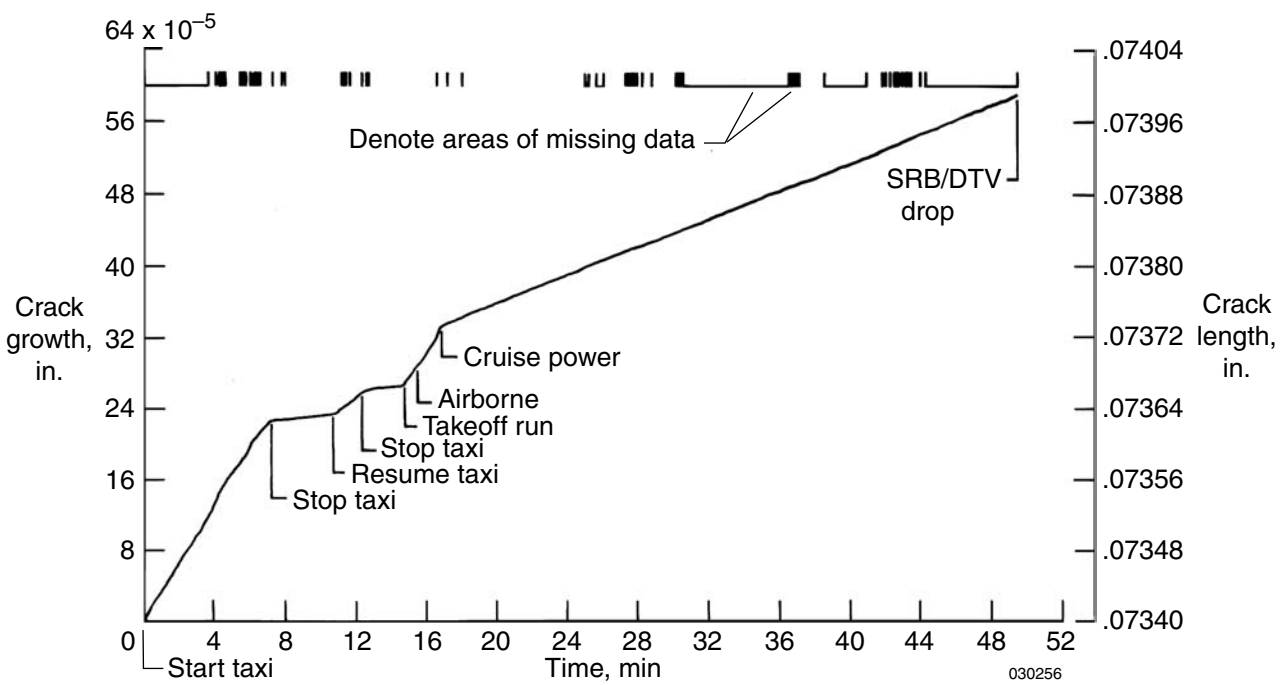

Figure 10. Crack growth curve for left rear hook (V_{BL}) critical stress point 2 (σ_2); B-52B carrying SRB/DTV.

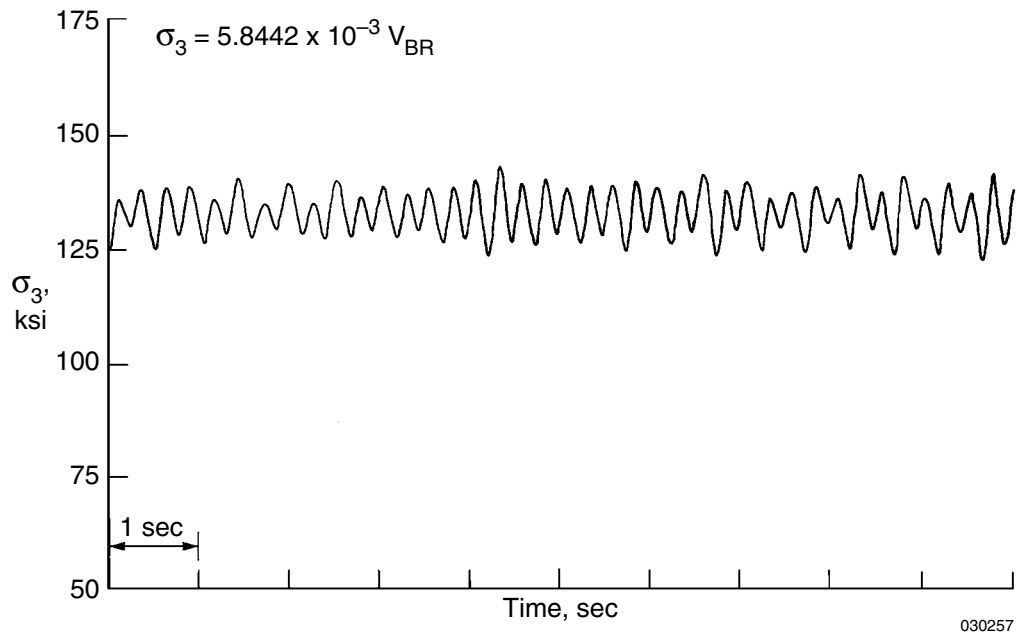

Figure 11. Typical random loading spectrum for right rear hook (V_{BR}) critical stress point 3 (σ_3); B-52B carrying SRB/DTV.

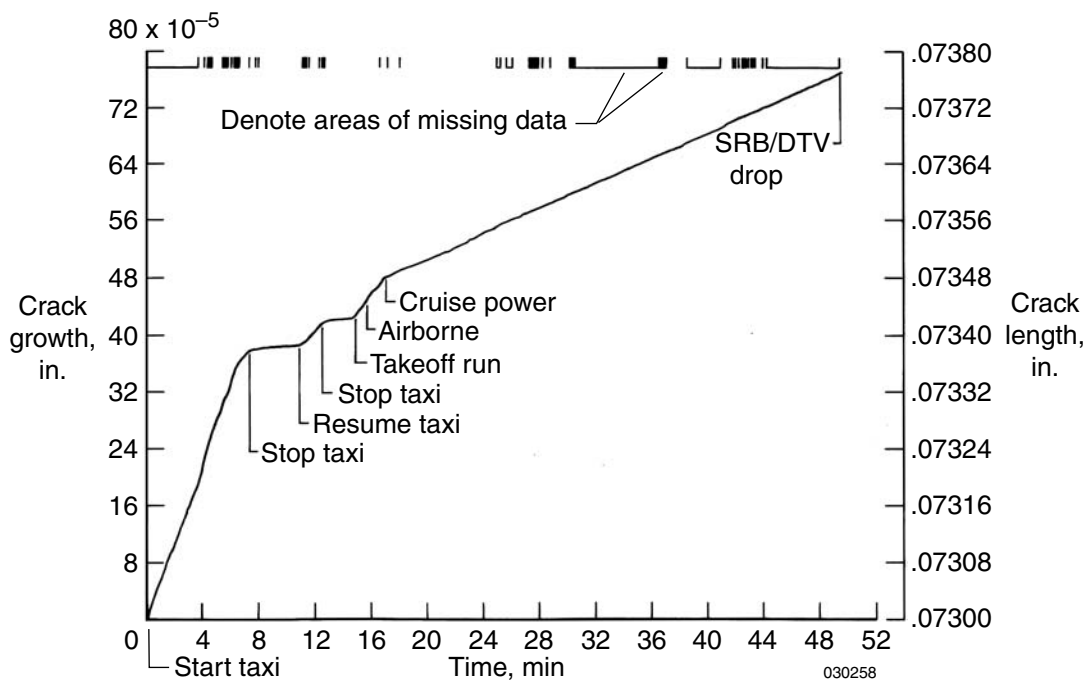

Figure 12. Crack growth curve for right rear hook (V_{BR}) critical stress point 3 (σ_3); B-52B carrying SRB/DTV.

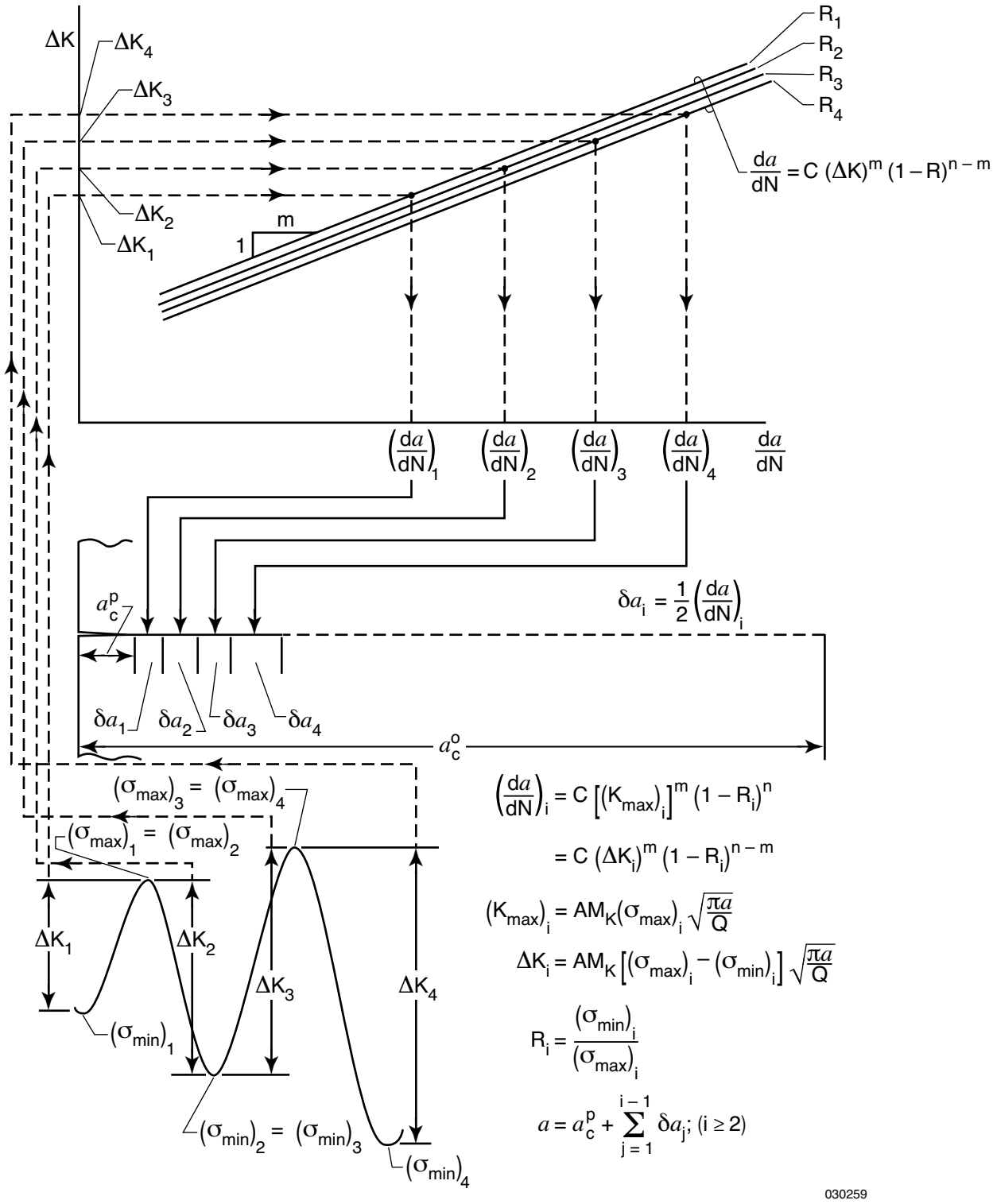

Figure 13. Graphic evaluation of crack growth increments for random loading spectrum using half-cycle theory.

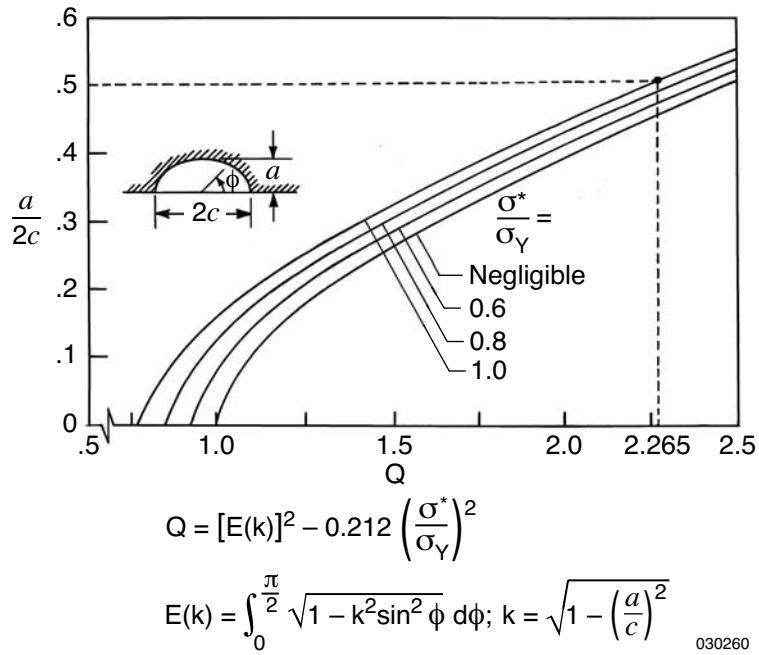

Figure 14. Surface flaw shape and plasticity factor for semi-elliptic surface crack.

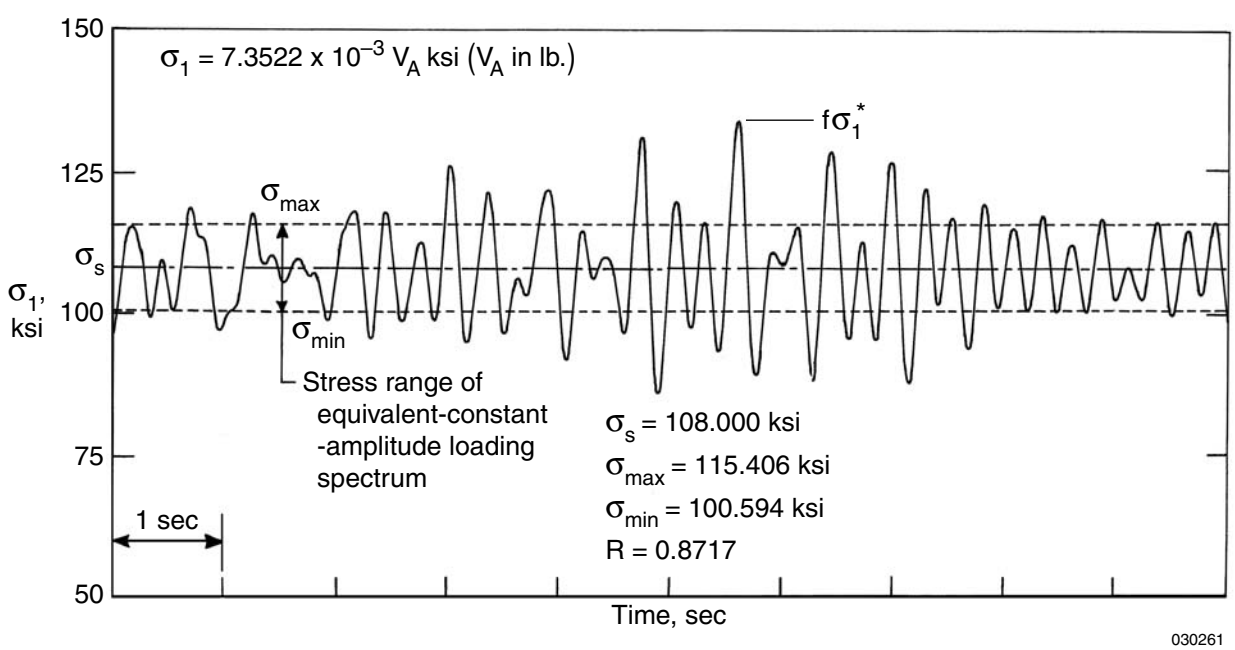

Figure 15. Representation of random loading spectrum with equivalent-constant-amplitude loading spectrum; front hook (V_A).

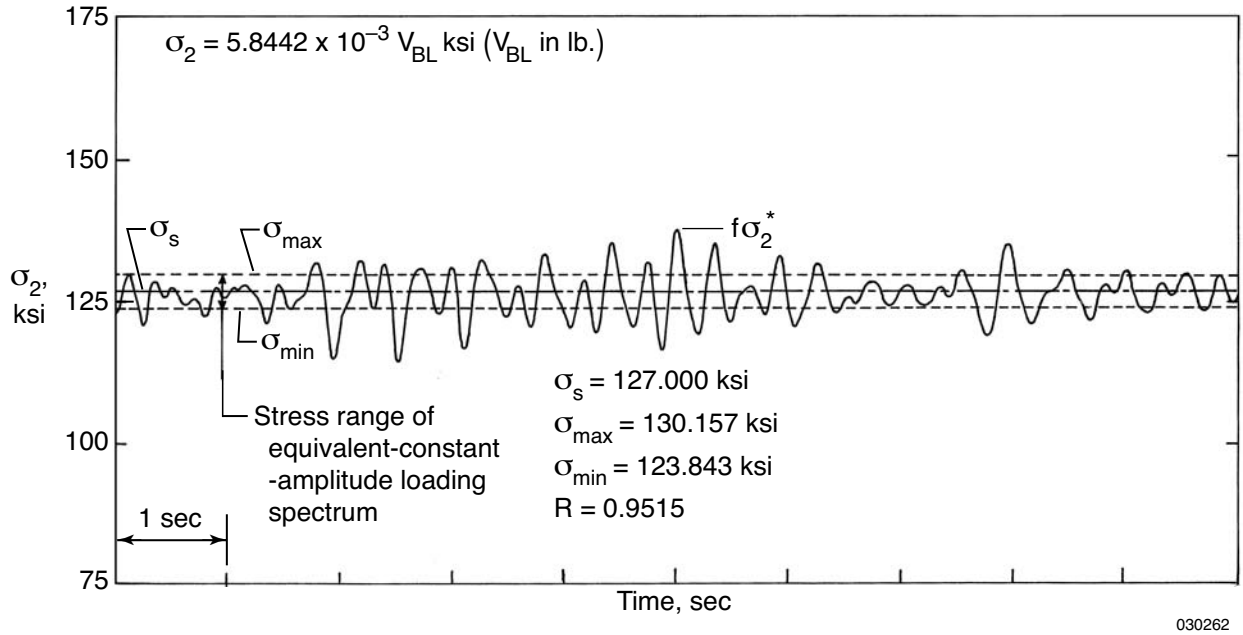

Figure 16. Representation of random loading spectrum with equivalent-constant-amplitude loading spectrum; rear left hook (V_{BL}).

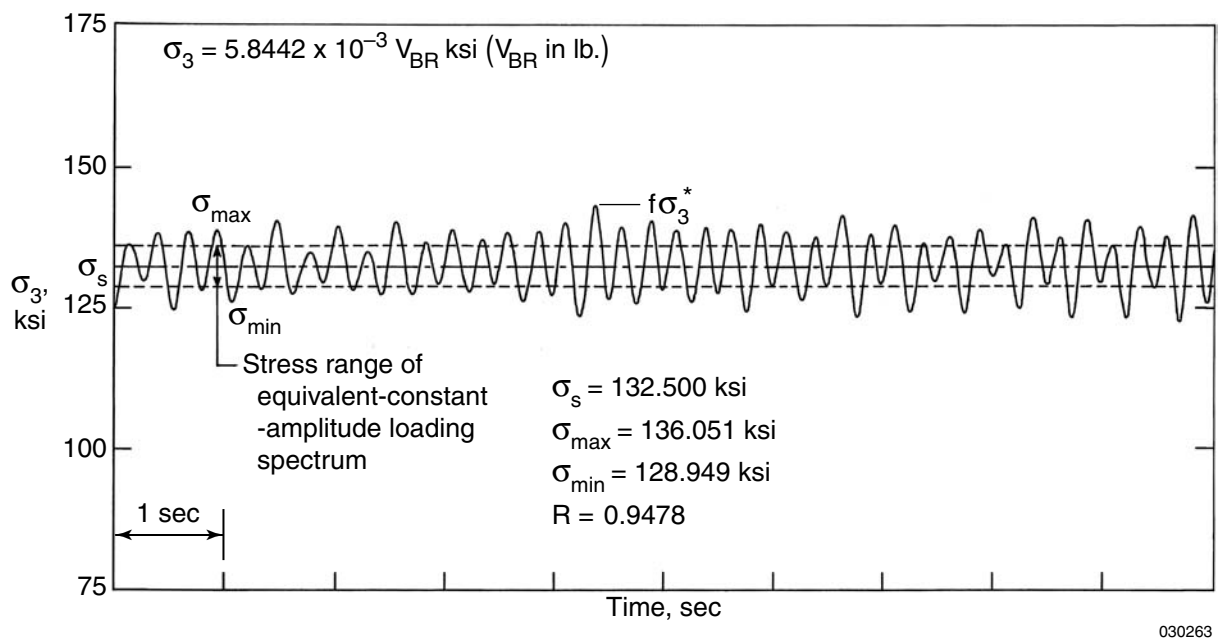

Figure 17. Representation of random loading spectrum with equivalent-constant-amplitude loading spectrum; rear right hook (V_{BR}).

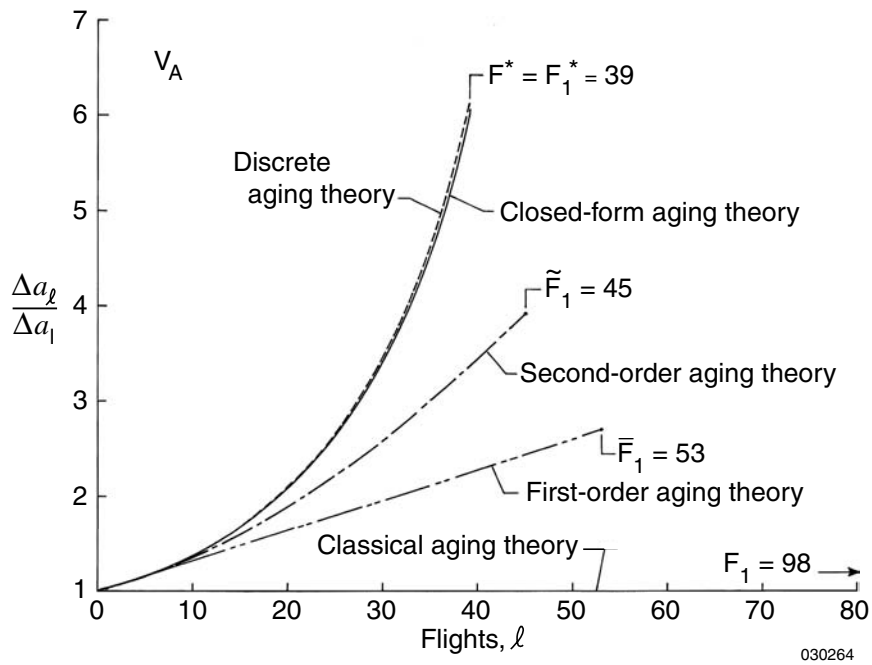

Figure 18. Crack growth ratio ($\Delta a_l / \Delta a_1$) curves calculated from different aging theories; front hook (V_A).

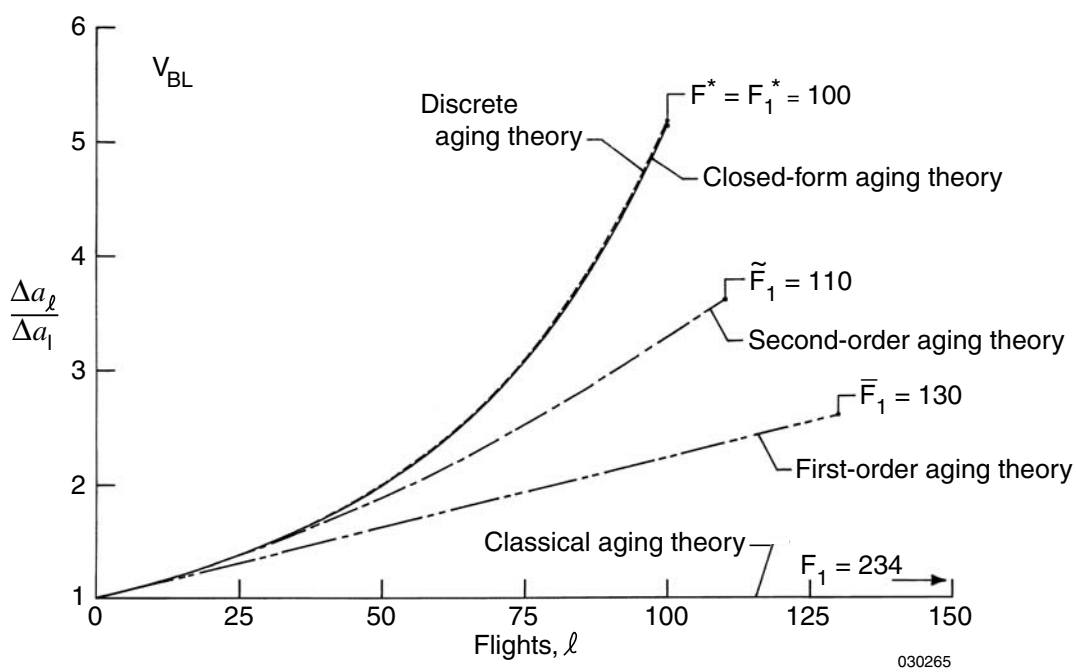

Figure 19. Crack growth ratio ($\Delta a_l / \Delta a_1$) curves calculated from different aging theories; rear left hook (V_{BL}).

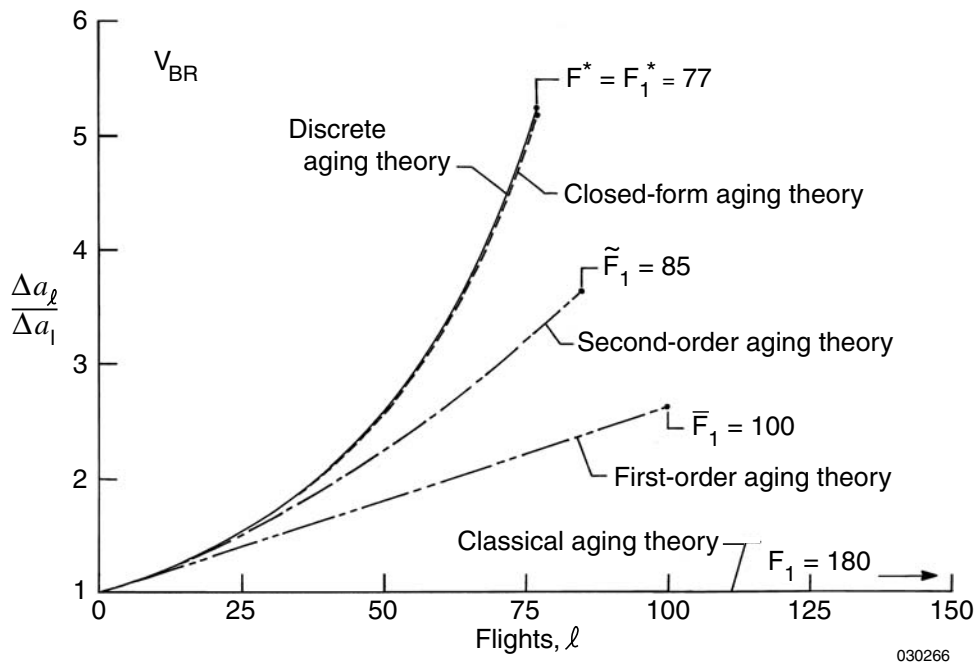

Figure 20. Crack growth ratio ($\Delta\alpha_l / \Delta\alpha_1$) curves calculated from different aging theories; rear right hook (V_{BR}).

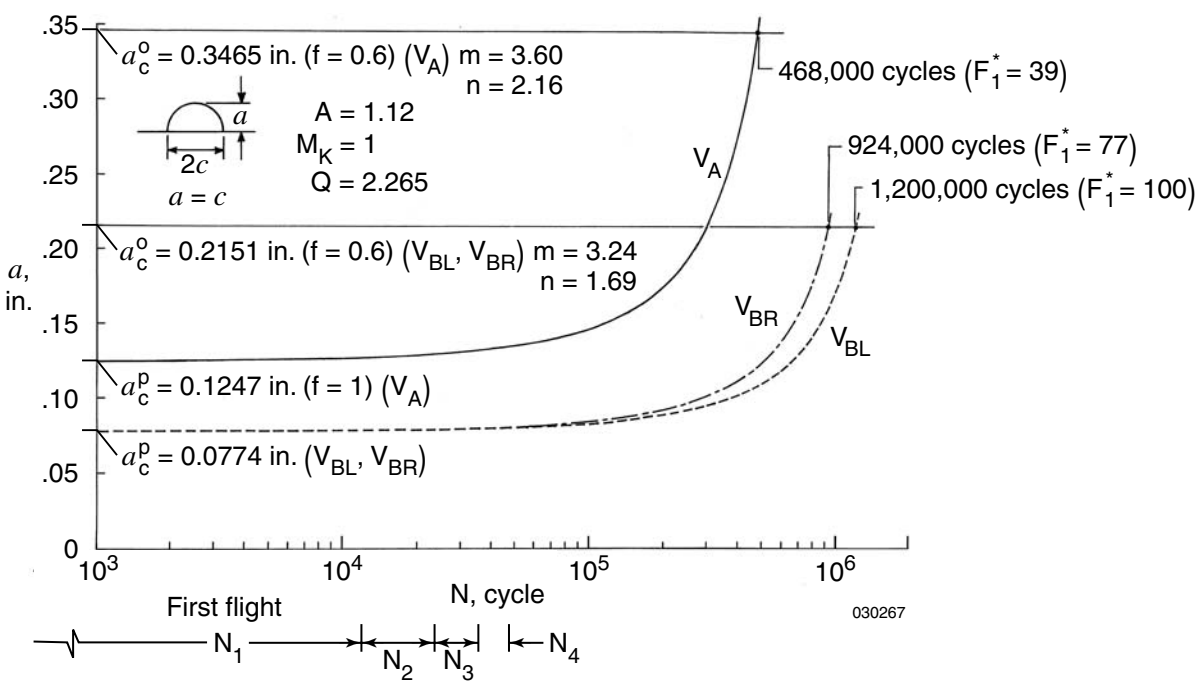

Figure 21. Crack growth curves in $a - N$ space calculated from closed-form aging theory for the front hook (V_A) and two rear hooks (V_{BL}, V_{BR}).

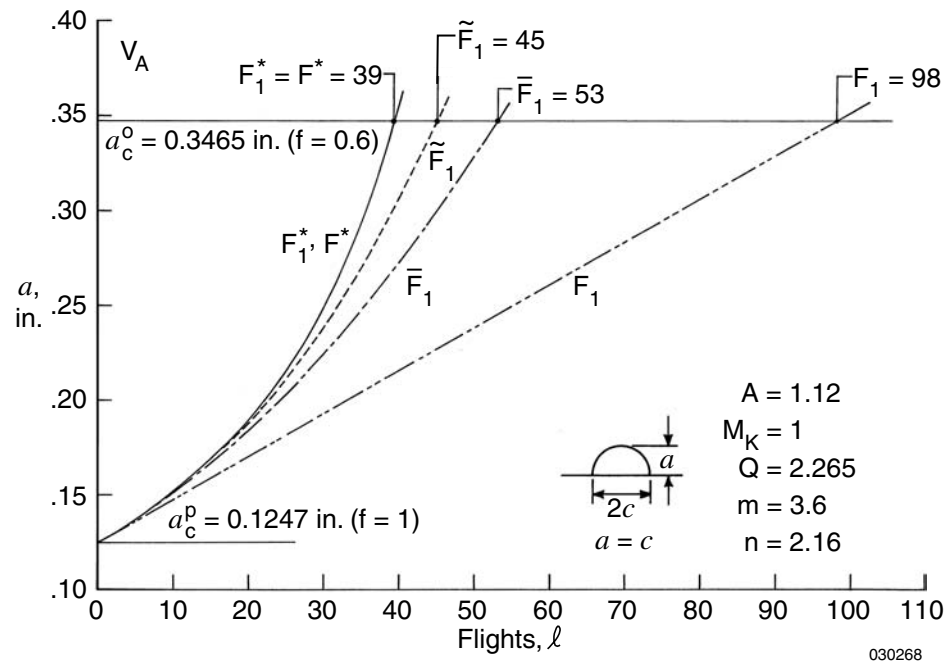

Figure 22. Crack growth curves in $a - flights$ space calculated from different aging theories; front hook.

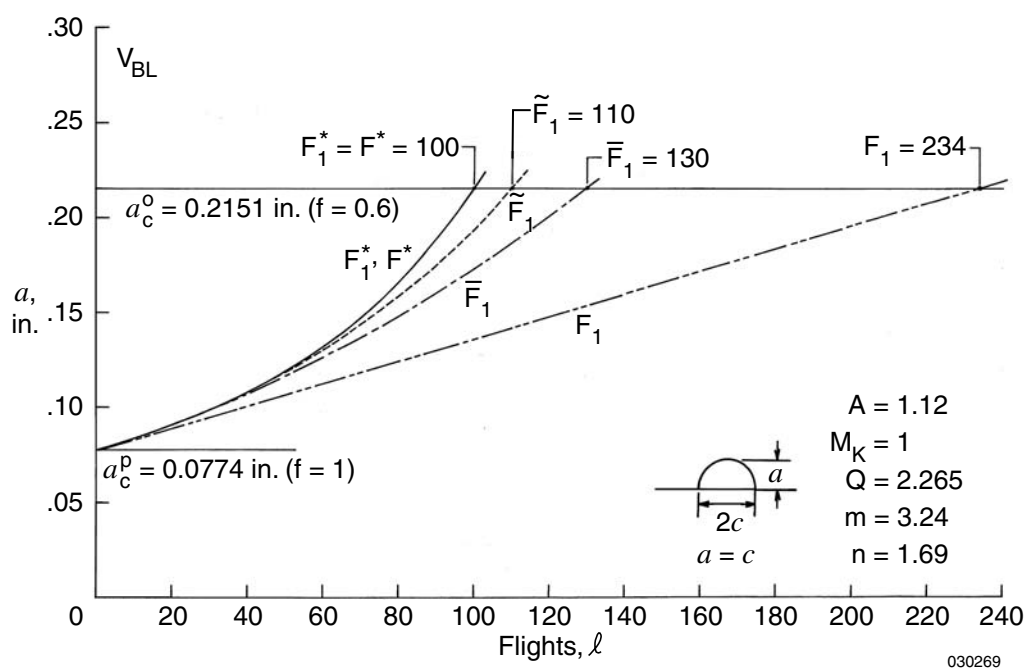

Figure 23. Crack growth curves in $a - flights$ space calculated from different aging theories; rear left hook.

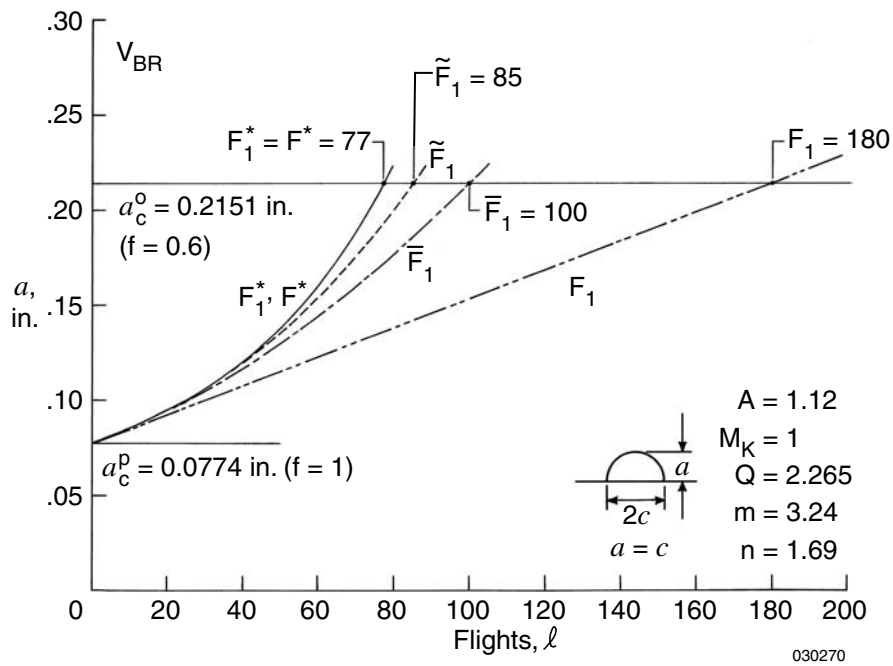

Figure 24. Crack growth curves in $a - flights$ space calculated from different aging theories; rear right hook.

REPORT DOCUMENTATION PAGE

Form Approved
OMB No. 0704-0188

Public reporting burden for this collection of information is estimated to average 1 hour per response, including the time for reviewing instructions, searching existing data sources, gathering and maintaining the data needed, and completing and reviewing the collection of information. Send comments regarding this burden estimate or any other aspect of this collection of information, including suggestions for reducing this burden, to Washington Headquarters Services, Directorate for Information Operations and Reports, 1215 Jefferson Davis Highway, Suite 1204, Arlington, VA 22202-4302, and to the Office of Management and Budget, Paperwork Reduction Project (0704-0188), Washington, DC 20503.

1. AGENCY USE ONLY (Leave blank)

2. REPORT DATE
December 2003

3. REPORT TYPE AND DATES COVERED
Technical Publication

4. TITLE AND SUBTITLE
Aging Theories for Establishing Safe Life Spans of Airborne Critical Structural Components

5. FUNDING NUMBERS
745-30-54-SE-35-00-52B

6. AUTHOR(S)
William L. Ko

7. PERFORMING ORGANIZATION NAME(S) AND ADDRESS(ES)
NASA Dryden Flight Research Center
P.O. Box 273
Edwards, California 93523-0273

8. PERFORMING ORGANIZATION REPORT NUMBER
H-2514

9. SPONSORING/MONITORING AGENCY NAME(S) AND ADDRESS(ES)
National Aeronautics and Space Administration
Washington, DC 20546-0001

10. SPONSORING/MONITORING AGENCY REPORT NUMBER
NASA/TP-2003-212034

11. SUPPLEMENTARY NOTES

12a. DISTRIBUTION/AVAILABILITY STATEMENT
Unclassified—Unlimited
Subject Category 39

This report is available at http://www.dfrc.nasa.gov/DTRS/

12b. DISTRIBUTION CODE

13. ABSTRACT (Maximum 200 words)

New aging theories have been developed to establish the safe life span of airborne critical structural components such as B-52B aircraft pylon hooks for carrying air-launch drop-test vehicles. The new aging theories use the “equivalent-constant-amplitude loading spectrum” to represent the actual random loading spectrum with the same damaging effect. The crack growth due to random loading cycling of the first flight is calculated using the half-cycle theory, and then extrapolated to all the crack growths of the subsequent flights. The predictions of the new aging theories (finite difference aging theory and closed-form aging theory) are compared with the classical flight-test life theory and the previously developed Ko first- and Ko second-order aging theories. The new aging theories predict the number of safe flights as considerably lower than that predicted by the classical aging theory, and slightly lower than those predicted by the Ko first- and Ko second-order aging theories due to the inclusion of all the higher order terms.

14. SUBJECT TERMS
Closed-form aging theory, Discrete aging theory, Equivalent constant stress cycle, Half cycle theory, Number of safe flights

15. NUMBER OF PAGES
41

16. PRICE CODE

17. SECURITY CLASSIFICATION OF REPORT
Unclassified

18. SECURITY CLASSIFICATION OF THIS PAGE
Unclassified

19. SECURITY CLASSIFICATION OF ABSTRACT
Unclassified

20. LIMITATION OF ABSTRACT
Unlimited